FLOW VISUALIZATION STUDY OF THE INTAKE PROCESS OF AN INTERNAL COMBUSTION ENGINE

by

Agop Ekchian

B.E. in Mechanical Engineering
American University of Beirut
(1973)

S.M. in Mechanical Engineering
Massachusetts Institute of Technology
(1976)

SUBMITTED IN PARTIAL FULFILLMENT
OF THE REQUIREMENTS FOR THE
DEGREE OF

DOCTOR OF PHILOSOPHY

at the

MASSACHUSETTS INSTITUTE OF TECHNOLOGY

(November. 1978)

Signature of Author .....
Department of Mechanical Engineering
November 15, 1978

Certified by.... .....
Thesis Supervisor

Accepted by.....
Chairman,
Department Committee on Graduate Students

FLOW VISUALIZATION STUDY OF THE INTAKE PROCESS OF AN INTERNAL COMBUSTION ENGINE

by

Agop Ekchian

Submitted to the Department of Mechanical Engineering on November 15, 1978 in partial fulfillment of the requirements for the Degree of Doctor of Philosophy.

ABSTRACT

The efficiency of combustion and the production of pollutants in the internal combustion engine are strongly dependent on the turbulent flow field in the engine cylinder. In most engines, turbulence is almost exclusively generated during the induction stroke. A water analog was used to visualize and study this process for a simple geometry cylinder.

The photographs of the flow that were obtained confirm the expected jet type flow through the intake valve, but demonstrate that this jet produces large toroidal vortex structures in the cylinder for certain operating conditions. These structures were shown to be of the same scale as the cylinder itself and very repeatable from cycle to cycle.

A detailed study of the characteristics of these toroidal structures was carried out for the case of an axisymmetric cylinder geometry. Inviscid scaling laws were obtained from the results that describe the development and stability of the structured flow field. It was also observed that small changes in geometry could have a significant effect on the induction process.

Thesis Supervisor: David P. Hoult
Title: Senior Research Associate
Sloan Automotive Laboratory

ACKNOWLEDGEMENTS

The author would like to express his gratitute to his advisor, Dr. David P. Hoult, for his guidance and interest during the course of this work. The author also wishes to express special thanks to Prof. John B. Heywood for his valuable support throughout the author's stay at M.I.T.

The author is also grateful to Dr. Joe M. Rife and Prof. Sheila E. Widnall for serving on his thesis committee and for their frequent and helpful suggestions.

Many thanks are also due to Messers. S. J. Albano, R. R. Fenner and D. F. Fitzgerald for their assistance in the construction of the experimental equipment and their interest in the project. The author also owes a debt of gratitude to the entire faculty, staff and students of the Sloan Automotive Laboratory for making the past five years a very positive experience.

This work was sponsored by the Department of Energy under contract number EC-77-S-01-5045. The author appreciates the valuable suggestions and criticisms of Dr. Peter O. Witze, the contract monitor.

TABLE OF CONTENTS

LIST OF TABLES

LIST OF FIGURES

NOMENCLATURE

ATC	after top dead center position
BDC	bottom dead center position
C_f	discharge coefficient
d_v	vortex core diameter
D_o	valve diameter
D_p	piston diameter
D_v	major diameter of vortex
L	nondimensional lift = $\frac{\text{valve lift}}{\text{valve dia.}}$
r	distance of a point from the closest point in vortex core (range: $o<r<d_v/2$)
R	nondimensional radius in vortex = $\frac{r}{R_p}$
R_p	piston radius
S.A.	valve seat angle
t	time
t_c	critical time for vortex breakup
u'	turbulence intensity
U	mean velocity in cylinder
V	velocity
V_p	piston velocity
X_p	piston displacement
δ	particle diameter
Θ	observed breakup angle
Θ_c	predicted breakup crank angle

ν	kinematic viscosity
ρ	density
ω	crankshaft
Ω	nondimensional angular velocity in vortex
$\vec{\nabla}$	del operator

I. Introduction

The structure of the turbulent flow field is a determining factor in the initiation, rate of propagation, and the efficiency of the combustion process in an internal combustion engine. The formation of a stable flame front, in a gasoline engine, is hampered by fluctuations in gas velocity in the immediate vicinity of the spark plug at the time of ignition.[1,2] This leads to the characteristic cycle-to-cycle variations in the cylinder peak pressure, which in turn causes a deterioration of engine performance. On the other hand, increasing the turbulence levels at the end of the compression stroke enhances the lean ignition limit and improves emissions.[3] Higher turbulence intensities inside the combustion chamber also lead to proportionally higher turbulent flame speeds.[4,5] This results in a more rapid rise in the temperature and pressure of the gas in the cylinder. These two quantities are closely linked to pollutant emissions and to the efficiency of combustion.

Therefore, the understanding of the turbulence in an automotive engine is critical for the success of present attempts to curb emissions and to improve

combustion efficiency. A great deal of effort has already been expended in an attempt to develop universal scaling laws for the turbulence in the cylinder. To date, the experimental data in support of these studies has been acquired primarily with hot-wire anemometers.

However, there are significant difficulties in using this technique to study the fluid mechanics inside an engine cylinder. The high relative turbulence intensities $\frac{u'}{U} > .2$, the highly unsteady nature of the flow, and the large pressure and temperature corrections that must be applied to hot-wire measurements (factors of 20 or more), make the results difficult to interpret. The most severe limitation of this technique, however, is that measurements can usually be obtained only at a single point in the flow field. This shortcoming is also true of the LDV (lasar doppler velocimeter) method. However, results obtained by some investigators indicate that the flow inside the cylinder may be anisotropic and nonhomogeneous, at least through the intake stroke and the early part of compression. [2,6,7]

Single point measurements of such a flow field are clearly inadequate. A complete picture of the flow structure can be obtained with the hot-wire technique

only if a matrix of measurement points covering the entire cylinder volume is used. Results of single point measurements are generally regarded by investigators to be only of qualitative value, and cannot be generalized to apply to different combustion chamber designs. In fact, the only universal conclusion that can be drawn with confidence about the nature of the turbulence in internal combustion engines is that intensity and mean velocity are linearly dependent on engine speed.[4,8]

However, experimenters have been able to demonstrate that, in engines without significant squish regions, turbulence is almost exclusively generated during induction.[6,9,10] An extensive volume of data has been generated in the study of this critical flow process and the consensus is that high shear flow during induction is the source of turbulence that is present in these engines. The high shear nature of the flow was demonstrated by using measurements that were obtained at several different locations in the cylinder by probes which could traverse the cylinder volume.[6,7]

However, the difficulty in interpreting hot-wire and LDV data has so far made it impossible to determine the structure of the flow field. Studies have led to the

opinion that the flow during induction must be structured[4,7,8], but no reliable picture of it has yet emerged. Such a picture is vital if a realistic fluid mechanic model of the flow during induction is to be developed.

The purpose of the experiment to be discussed here was to visualize the flow during the important induction process so as to observe the structure as a whole and obtain a complete picture of the flow field. The photographs of the flow that were obtained confirm the expected jet type flow through the intake valve, but demonstrate that this jet produces large toroidal vortex structures in the cylinder for certain operating conditions. These structures were shown to be of the same scale as the cylinder itself and very repeatable from cycle to cycle.

Past experiments have shown that parameters such as valve lift, valve seat angle and the distance between the valve and the cylinder wall have an important effect on the flow through the intake valve opening.[11,12] These parameters affect the discharge coefficient of the intake valve and thus determine the maximum density of charge that can be obtained in the engine cylinder at the end of induction. This visualization experiment shows

that these quantities have a more far-reaching influence. They not only alter the flow in the immediate vicinity of the valve throat, but also have a signficant effect on the entire flow field of the cylinder volume during the whole induction process.

A water analog was used for visualization purposes in this experiment. The study deals mainly with the intake process in an axisymmetric cylinder with a centrally located intake valve. This idealized case was chosen because it was possible to identify and analyze the important flow characteristics. Similar flow structures were shown to exist in a more conventional geometry, but were too complicated to be analyzed even by this visualization technique.

Other visualization methods such as Schleiren and shadowgraphy exist which can be used in an actual engine; but they are not well-suited for the study of flows, such as the intake process, where density gradients are minimal. These methods also have the drawback that the image obtained is integrated over a line of sight which passes through a very complicated flow field.

However, no visualization technique can be expected to replace LDV or hot-wire anemometry in the study of

turbulent flows. It can only be used to enhance the understanding of results obtained by these techniques by reducing the guesswork that is now necessary. For example, the appreciation of the flow structure would alleviate the directional ambiguity of the hot-wire anemometer and also enable investigators to choose more strategic locations for point measurements.

II. Apparatus

The mechanism that was used in this experiment is shown schematically in Fig. 1. The fluid used was distilled water and the flow was visualized in the plexiglass cylinder shown. In order to be able to photograph the flow with a minimum of distortion, it was necessary to fit the cylinder into a plexiglass box that was also filled with water.

Water was forced into the visualization cylinder by a hydraulic actuating piston via flow straighteners (Fig. 1). Water was not pulled into the plexiglass cylinder by suction so as to avoid cavitation problems that would occur at the valve throat during high speed operation.

A 3.19 in. (8.1 cm.) diameter piston was used for all the experiments, and the clearance volume of the cylinder was maintained at 3.3 $in.^3$ (54 $cm.^3$). The piston stroke was varied for the different experimental cases by changing the crank radius of the crankshaft. The range of bore-to-stroke ratios chosen for these experiments (.74 to 1.35) brackets values encountered in most production and experimental engines.

The actuating cylinder was powered by a variable speed d.c. motor (3 H.P., 1750 RPM max.) via a reduction gear

and a slider crank mechanism. The coupling was designed so that the slave piston in the plexiglass cylinder would travel through one induction stroke each time the mechanism was actuated. The piston had to be manually returned to its top center position before the next experiment.

The cylinder head was flat and was designed to accommodate different valve locations and valve seat angles. Details of the valve and valve seat geometry are given in Fig. 2. The valve diameter to piston diameter ratio of .45 is a commonly observed value in production engines. The intake valve also remained stationary at a preset opening during the entire induction process.

The photographs of the flow field were taken by means of either a Crown Graphic, 4 x 5 format, still camera or a Red Lake Hycam movie camera (range of operation 40 to 1,000 frames/sec.). Time reference marks were obtained on the movie film by triggering a neon timing light in the camera at every five degrees of rotation of the engine crankshaft. A Trump-Ross pulse generator was mounted on the d.c. motor shaft and was used to trigger the neon bulb.

The films used were Polaroid type 57 in the still camera and Kodak 4X reversal and Kodak 2484 negative in the Hycam camera. Four General Electric DMD light bulbs were used as the light source for the experiment.

III. Experimental Procedure

A water model was used in this experiment, instead of attempting to visualize the actual gas flow in an engine cylinder, because of two basic considerations. First, by using water it is possible to greatly reduce the velocities involved in the experiment and thus significantly simplify data acquisition. Second, and perhaps the more important reason for resorting to this model, is that no appropriate tracers exist that can be used effectively with air.

This experimental model was scaled by maintaining geometric similitude and a Reynolds number, $\frac{V_p D_p}{\nu}$, equivalence based on piston velocity, V_p, and piston diameter, D_p. Since the angular velocity of the crankshaft, ω, is directly proportional to the piston velocity, the Strouhal number, $\frac{\omega D_p}{V_p}$, was automatically matched in this experiment. A more extensive discussion of the scaling of this problem is given in Appendix A.

For the kinematic viscosity, ν, in the Reynolds number calculation, the temperature of the intake air for an engine cylinder was assumed to be 150°F (66°C), while the temperature of water in the experiment was 70°F (21°C). Consequently, velocities in the model were scaled down by a factor of 17:1 from those commonly observed in reciprocating engines.

Fig. 3 is a plot of the approximate Mach number, at the valve throat, during the intake process of a typical production engine with dimensions similar to those of the model. These values were calculated using incompressible flow equations with actual valve lift profiles. However, the reverse flow through the intake valve, that normally occurs during the early part of induction, was neglected.

It is clear that during intake, Mach numbers at the valve throat, the point of maximum velocity, are generally lower than 0.3. Since this is the commonly accepted threshold for neglecting compressibility effects, the water model should be a valid analog of the actual flow field. In fact, if reverse flow had been considered, the Mach numbers at the early part of the induction stroke would have been even lower.

For the bulk of the test conditions in this experiment, polystyrene pellets, were used as tracers to visualize the flow. These spherical pellets were almost neutrally buoyant (1.01 to 1.04 specific gravity) and ranged in diameter from .02" to .03" (0.5 mm to 0.8mm) or from .03" to .04" (0.8 mm to 1.0 mm), depending on the experiment. The larger pellets were used for the faster speeds since more reflected light was necessary. For these experimental conditions, only a single .25 in. (.63 cm)

thick plan parallel to the axis of the cylinder was illuminated at a time. Pictures of the flow were taken at 90° to this plane. A schematic of this technique is shown in Fig. 4. Of course, only the pellets that are in this illuminated zone, indicated by open circles in the figure, can reflect any light and be recorded by the camera. Since the thickness of the illuminated zone was only 8 percent of the total cylinder diameter, the photographs obtained are essentially a record of only one plane of the motion. It was necessary to study one plane at a time because of the complexity of the flow field.

The photographs obtained in this way were used to determine the structure of the flow, obtain velocity measurements, and also obtain particle trajectories.

Velocity measurements were made by measuring streak lengths left by the tracer particles on the photographic film. The lengths of these streaks, which were controlled by adjusting the exposure time of the camera, corresponded to one or two crank angle degrees of rotation of the driving crankshaft.

Particle trajectories, on the other hand, were measured by filming at high enough speeds so that particles could not travel too far between frames of the movie. Consequently, the motion of each particle could be followed

over a significant number of crank angles. Exposure times used in these cases corresponded to approximately 0.2 crank angle degrees.

The effectiveness of using polystyrene pellets as tracers to obtain velocity measurements has been tested by experimenters. Allen and Yerman report an error of only 2-4 percent, for moderate flow velocities (3-6 ft./sec.), by comparison to pitot tube measurements.[13] Roberson predicts a 3-8 percent deviation of the path of a polystyrene sphere (1 mm in diameter and a specific gravity of 1.05) from the streamlines of highly swirling flows that are commonly observed in combustion systems.[14] In the highly complex flow field of this experiment, however, the error was estimated from the photographs to be approximately 10 percent. This was accomplished by comparing velocities, at the valve throat, measured from the photographs with calculated values. This was sometimes possible when particles entered the intake jet near the valve opening where velocities are approximately known.

Accuracy of this method could be increased dramatically by using smaller diameter polystyrene pellets.[14] However, smaller size tracers are difficult to photograph and the size of the particles used in these experiments could not be reduced without a serious deterioration in the quality

of the resulting pictures.

The response time of a typical particle, used in this experiment was calculated for a step rise in fluid velocity of 15 in./sec. (typical piston velocity at high speeds). An empirical drag coefficient for a sphere undergoing an unsteady motion (see Appendix B) was used to calculate the force on the polystyrene pellets.[27] It was found that a pellet, under these conditions, would accelerate from 10 percent to 90 percent of the fluid velocity in 16 milli sec. (this corresponds to 16 crank angle degrees at 2500 scale RPM and 4 crank angle degrees at 750 scale RPM).

On the other hand, a rise time (the time it takes for the intake velocity to increase from 10 percent to 90 percent of its peak value) of .06 seconds was calculated for the velocity at the valve throat at 2500 scale RPM. This is approximately four times larger than the response time of the particle above. Consequently, the response of the tracing particle is adequate for tracing the relatively slow accelerations of the bulk flow even at the highest RPM considered.

However, these particles are too large to respond to the higher frequency turbulent eddies. In fact, Faure estimates that to adequately study turbulence, it is necessary to use significantly smaller particles (~.01 mm).[16]

Such small particles were not used here because they could not be photographed satisfactorily.

Fig. 5, a sample photograph which was obtained by this technique, shows the streaks which mark the paths of the particles. The lack of ripple in these paths is not an indication of the absence of turbulence, but reflects the inability of the particles used here to respond to the small scale oscillations. In fact, the Reynolds number of the flow based on mean piston velocity and diameter ranges from 7,500 to 25,000 for the range of RPM's considered.

Finally, in another set of tests, air bubbles introduced into the cylinder were used as tracers instead of polystyrene spheres. In these cases the entire cylinder was illuminated.

IV. Test Matrix

The test conditions in this experiment were chosen so as to determine the fundamental properties of the flow in an internal combustion engine. In order to observe these properties without unnecessarily complicating the flow, a simplified axisymmetric geometry cylinder with a stationary intake valve was used.

Table I shows an outline of the experimental operating conditions. Three of the parameters shown, RPM, bore-to-stroke ratio and valve lift were studied in detail for their effect on the flow field structure. The effects of the valve seat angle and valve location were also investigated, but this analysis was of a qualitative nature.

In all but the eighth test condition, the axisymmetric cylinder geometry was used. In these cases, it was only necessary to study one axial plane of the cylinder since the entire flow field could be described by the revolution of any such plane about the axis.

The effect of the Reynolds number of the intake jet, which is proportional to piston velocity, was investigated in the first three cases shown in Table I. This investigation was performed at two different bore-to-stroke ratios and three different RPM's.

Test #	RPM	$\frac{\text{Bore}}{\text{Stroke}}$	L	S.A.	Valve location
1a) Effect of RPM	750	1.35	.21	45°	axisymmetric
1b) " " "	750	1.06	.21	45°	"
2a) " " "	1500	1.35	.21	45°	"
2b) " " "	1500	1.06	.21	45°	"
3a) " " "	2500	1.35	.21	45°	"
3b) " " "	2500	1.06	.21	45°	"
4) Effect of Stroke	750	.74	.21	45°	"
5a) Effect of Lift	750	1.35	.07	45°	"
5b) " " "	750	1.06	.07	45°	"
6) Effect of Valve Angle	750	1.06	.21	60°	"
7a) " " "	750	1.06	.21	30°	"
7b) " " "	750	1.06	.07	30°	"
8) Effect of Valve Location	750	1.35	.21	45°	off-center
9) Air Bubble Technique	345	.74	.07	45°	axisymmetric

Table I: Test Matrix

A range of bore-to-stroke ratios was used in this experiment because of the correlation that was observed between the stability of the structured flow field and the position of the piston in the cylinder. Test #4, in conjunction with tests 1a and 1b, bracket the values of bore-to-stroke ratio that are encountered in most automotive engines.

Since a stationary valve was used in this experiment, test #5 was performed to study the effect of the small lifts that are encountered during the early part of induction in actual engines. Valve lift is defined as the axial distance moved by the valve stem from its fully closed position. The range of dimensionless lift L (valve lift/ valve dia.) that was used here is the range of operation commonly encountered.

The next two cases, nos. 6 & 7, were qualitative investigations of the effect of changing the valve seat angle (indicated as S.A. in Fig. 2).

In case #8, the experimental apparatus was fitted with a more conventional offset intake valve. This resulted in a much more complicated induction process, but comparisons were possible with the simpler geometry. Because the flow was no longer axisymmetric, two perpendicular planes (shown in Fig. 6) were photographed.

Finally, case #9 was performed without the polystyrene tracers. In this case, air bubbles were introduced into the visualization cylinder which allowed a different aspect of the flow, its stability, to be studied. Only in this test was the entire flow field illuminated and studied as a whole.

It should be noted that each test in Table I was repeated several times. Where data from different runs of the same test condition are reported, they are differentiated by lower case Roman numerals.

V. Results and Discussion

The photographs of the visualization of the induction stroke in the axisymmetric cases (unless otherwise indicated, the discussion will be restricted to the axisymmetric cases) indicate the presence of a structured flow that is comprised of two toroidal vortices. This flow field is shown in the photograph in Fig. 5, while the schematic in Fig. 7 shows the ring shaped axes of rotation of the two vortices.

These two rings are formed early in the induction stroke as the intake flow separates at the valve and the valve seat. The upper vortex, shown in Figs. 5 and 7, is approximately located in the clearance volume of the cylinder. It is trapped in its position by the conical intake jet and remains constant in size and location. The lower vortex, also shown, is a moving vortex which fills the piston swept volume. When formed it has a major diameter, D_V, approximately equal to the diameter of the valve. As the piston moves through its stroke, this vortex follows the motion of the piston at half the speed and grows in both its major and minor diameters.

The major diameter, D_V, of either vortex ring is defined as the distance between the two points of

intersection of the axis of rotation of the vortex and an axial plane of the cylinder. The minor diameter, d_v, is the diameter of the core of the vortex and is roughly a measure of the amount of the fluid that rotates about one center of rotation in the axial plane. It is difficult to determine the value of d_v of the lower vortex from the photographs. This is especially true for the long stroke configurations where the vortex has an oval shape late in the stroke.

These vortices also develop azimuthal oscillatory instabilities in their cores. This instability, in the lower vortex, grows with time and under certain conditions leads to a breakup of the structured flow field. This behavior is not observed in the upper vortex.

A) Reynolds number effect on flow structure - An increase in crankshaft speed results in an increase in the intake jet Reynolds number and a proportional decrease in the time taken by the induction process. Figs. 8a and 8b are photographic comparisons of the flow field for three different cases (1a, 2a and 3a) where the RPM and consequently the Reynolds number are increased by a factor of 3.5. All the photographs are taken at a bore-to-stroke ratio, B/S, of 1.35 and a dimensionless

lift of .21. The crank angle degrees from the top dead center position of the intake stroke are noted on the left-hand side of each row while each column represents data from a single RPM.

The most striking feature of these photographs, besides the structure of the flow, is the similarity of the flow field for the three different test conditions. The only parameters that are changed are camera shutter speed and RPM of the crankshaft.

The growth of the lower vortex major diameter as a function of piston position is shown graphically in Fig. 9. Vortex diameter and piston position are made dimensionless by dividing by valve and piston diameters respectively. It can be seen that D_v initially has a value approximately equal to the valve diameter and asymptotically approaches a value 50 percent larger. This behavior is independent of RPM, or Reynolds number, within the scatter of the data and is only a function of dimensionless piston displacement.

Similarly, Fig. 10 indicates the independence of the moving vortex position, X_v, from crank speed. In fact, if the X_v is made nondimensional by dividing by piston displacement X_p, the figure indicates that the vortex is always halfway between the piston position at a given

time and the position of the piston at top dead center.

Fig. 11 is a log-log plot of the nondimensional angular velocity distribution in the lower vortex, Ω, as a function of the nondimensional position, R, for a scale RPM of 750. Ω, is defined as angular velocity at a given point in the lower toroidal vortex divided by crankshaft angular velocity, ω, while R is defined as the shortest distance from that point to the axis of rotation of the vortex divided by the radius of the piston R_p. This figure shows the results of angular velocity measurements in the lower vortex for several different crank angles. It should be noted, however, that data presented was obtained from two or three executions of the induction process (indicated by lower case Roman numerals) without having varied any of the parameters.

It can be seen in Fig. 11 that the data from several tests and many different crank angles falls within a narrow band about a single line defined by:

$$\Omega = \frac{2.7}{R^{1.2}} \qquad R \neq 0 \qquad [1]$$

Figs. 12 and 13 demonstrate that this behavior, which can also be observed for the higher speeds of 1500 and 2500 RPM, is independent of Reynolds number.

From Eq. 1 it is possible to calculate a nondimensional vorticity distribution

$$W = \frac{1}{R} \quad \frac{\partial(R^2\Omega)}{\partial R} \qquad R \neq 0 \qquad [2]$$

if it is assumed that the streamlines are concentric circles about the axis of rotation of the vortex.

The resulting distribution

$$W = \frac{2.17}{R^{1.2}} \qquad [3]$$

is shown in Fig. 14. It can be seen from the figure, which is applicable to all three RPM's, that the distribution of vorticity in the lower toroidal vortex is highly peaked at the center of rotation. In fact, it is demonstrated in Fig. 11 that the outer regions of the vortex (within the scatter of the data) have a velocity profile that is similar to a free vortex distribution given by:

$$\Omega = \frac{1.25}{R^2} \qquad [4]$$

Figs. 11, 12 and 13 also show that the process is very repeatable. At a fixed R, there is not a significant amount of cycle-to-cycle variation in angular velocity over many cycles. Perhaps more importantly, however, the angular velocity at a fixed point in the vortex is also relatively constant with time or crank angle. This

indicates that, once the vortex is formed, there is not a significant amount of dissipation in the time scale of one cycle. In fact, it is possible to show (see Appendix C) that at the BDC position the lower vortex may still retain as much as 40 percent of the total mean flow kinetic energy that entered the cylinder up to that point.

At this point, three deductions may be made about the flow field in the engine cylinder: 1) The most obvious conclusion is that the velocity distribution in the lower vortex, just like vortex diameter and vortex location, is independent of Reynolds number for the range of speeds considered. 2) The flow is not only structured, but repeatable. 3) Vortex angular velocities inside a given vortex are constant with time or crank angle. This is an indication that the velocity and consequently energy are conserved by this lower vortex.

The data presented thus far indicates that simple scaling laws can be used to describe the development (position and size of toroidal vortices) and velocity distribution in the structured flow field of this model. However, it was discovered that the lower vortex, which occupied the piston swept volume, had inherent instabilities which resulted in its breakup under certain conditions.

B) Vortex instability and breakup - One of the operating conditions which resulted in the breakup of the structured flow over most of the cylinder volume was the long stroke.

The effect of changing this parameter is demonstrated in Figs. 15a and 15b. All the pictures in these two figures are taken at a RPM of 750 and a dimensionless valve lift of .21, while each of the three columns represents a different bore-to-stroke ratio. For the short and medium strokes, the two toroidal vortices were present throughout the entire induction process. Extending the stroke (case 4, Table I) results in a similar flow field during the early part of induction (Fig. 15a, left column). However, the lower vortex begins to degenerate rapidly as the piston passes a critical position (approximately where the piston displacement equals the bore) and at bottom dead center, BDC, the structure is no longer visible (Fig. 15b, left hand column).

This instability phenomenon is observed more easily in Figs. 16a and 16b. Here, only air bubbles were used as tracers and the entire cylinder was illuminated. Air, being significantly lighter than water, was forced to the center of the rapidly spinning flow, due to centrifugal

force. Consequently, the axes of rotation of the two ring vortices were made visible without any interference from the rest of the flow field. The sequence of pictures 'a' through 'h' demonstrates the shape and position of these axes at different points in the stroke up to the point where the lower ring is destroyed.

Azimuthal oscillations are observed along the axes of both rings almost as soon as they are formed. While these oscillations do not change in magnitude in the upper vortex, they grow with time in the moving ring. When the displacement of the piston is approximately equal to the bore, the lower ring is seen to burst into a totally random flow.

The development of the toroidal vortices in this experiment and the azimuthal oscillations observed along the cores are remarkably similar to the behavior of unbounded ring vortices, which have been studied extensively by many investigators (see Refs. 17 through 22).

Until this breakup occurs, however, the flow field is the same in the long and short stroke configurations. The similarities in vortex position and diameter for these cases are shown in Figs. 9 and 10. Figure 17 shows that the velocity profile still lies on the curve defined by

Eq. 1; however, in this case a factor Y is applied to Ω.

$$\Omega Y = \frac{2.7}{R^{1.2}} \qquad R \neq 0 \qquad [5]$$

Y is the length ratio of the strokes in the short and long stroke cases (Y = .55) and compensates for the higher mean piston velocity of the long stroke configuration.

The onset of a similar instability was observed due to decreasing the valve lift. Figures 18a and 18b demonstrate the effect of decreasing the lift (L = .21) by a factor of 3. Again the flow develops in the same manner for both conditions, but in the case of the smaller valve opening it soon passes a critical point and the lower ring is destroyed.

The similarity in vortex development, which can be observed in the pictures from the two cases, is also demonstrated in Figs. 9 and 10. The size and location of the lower vortex is not a function of valve lift.

It was found that the velocity distribution for the smaller valve lift, shown in Fig. 19, could again be described by Eq. 1 if a factor Z was applied the dimensionless angular velocity Ω

$$\Omega Z = \frac{2.7}{R^{1.2}} \qquad R \neq 0 \qquad [6]$$

This factor, which compensates for the expected increase in flow velocity due to the decrease in valve flow area,

is equal to the effective area ratio for the two cases. This ratio is the product of the geometric flow area and discharge coefficient ratios for the two valve lifts. The value of Z, which was determined experimentally to be .58, indicated that the discharge coefficient for the lower valve lift was approximately 70 percent larger. Similar variations in discharge coefficient as a function of valve lift have been observed by other experimenters.[11,23]

It should also be noted that, in an actual engine where the valve gradually opens during the induction process, the velocities will be closer to those observed in Fig. 19 early in the stroke and those in Fig. 11 late in the stroke. This would probably result in a velocity distribution that would be closer to the free vortex line shown in Fig. 11.

It is important to note that the instability in this case occurred at a point in the cycle before the piston displacement equaled the piston bore. Consequently, piston position is not the only governing parameter in the lower vortex breakup.

It was found that the instability of the lower vortex was in fact a function of the strength (circulation) of the lower vortex and the duration of the stroke. A

nondimensional parameter

$$K = \frac{\Gamma t}{D_v^2} \qquad [7]$$

can be defined which incorporates these two effects. In this equation, Γ is the circulation of the vortex calculated from the Ω vs. R curves at R = .5, while 't' is the duration of the intake stroke. The value of R = .5 was chosen because beyond this point the circulation did not change significantly, and at R = .5 the vortex filled the diameter of the cylinder.

The values of K are shown in Table II for several of the experimental cases that were studied for the breakup phenomenon. Each breakup crank angle, θ, shown in this table is an average value of the observed breakup points. These points were obtained by studying movies of several identical runs.

The breakup of the vortex in the first experiment in Table II occurred at approximately 174 crank angle degrees after the start of induction. The time for this portion of the stroke was used to determine a critical value $K_c = 48$ at which point breakup occurred in this case.

It can be deduced from Table II that structured vortex flow persisted throughout the entire induction

RPM	STROKE	LIFT	K	θ	θ_c
750	1.06	.21	50*	174	174
1500	1.06	.21	50	186	174
2500	1.35	.21	37	249	236
2500	1.06	.21	50	160	174
750	.74	.21	69	128	125
750	1.35	.07	66	136	131
750	1.06	.07	90	102	97

*base condition

Table II: Observed and Predicted Crank Angle of Vortex Breakup.

process only when the value of K was less than 48.

In order to test K as a criterion for vortex breakup, a critical time, t_c, for the breakup was calculated

$$t_c = \frac{K_c D_v^2}{\Gamma} \qquad [8]$$

for each case. From these values, a predicted breakup crank angle, θ_c, was calculated for each test condition (Table II). The close agreement between observed values of the breakup, θ, and the predicted values, θ_c, indicates that K, essentially a critical time ratio

$$K = K_c \frac{t}{t_c} \qquad [9]$$

is an appropriate measure of the stability of this flow field.

Consequently, any parametric change which increases the strength of the lower vortex, such as increased stroke length or decreased valve lift, will hasten the destruction of the structured flow. Simply increasing RPM also increases the circulation, but in this case the time taken by one stroke is proportionally shorter, and the critical crank angle does not change. The vortex in each experimental case has a characteristic lifetime. The structured flow can survive into the compression stroke only if the duration of the induction process is shorter than this characteristic time.

This inviscid instability is very similar to the results observed by experimenters in the study of unbounded vortex rings. In these experiments a slug of fluid was ejected from an orifice and its motion was observed as it traveled in an unbounded region. It was found that these vortices became unstable approximately five diameters (diameter of the vortex generating orifice) downstream from the point where azimuthal waviness developed in the core.[18]

In this experiment, the vortex is surrounded by rigid boundaries and it cannot travel freely as in the unbounded cases. But it was possible to calculate a self-induced velocity from the measured parameters and to determine a critical breakup time based on this theory (see Appendix D). The results showed remarkable agreement. The number of azimuthal waves that were observed in the core of the vortex in this experiment also conformed to the theory which was developed for the unbounded rings (Appendix D).

The upper, stationary vortex has not yet been discussed primarily because it represents a small portion of the flow. It also has a much less exciting history. It does not change in size or location significantly throughout the entire induction stroke. It exhibits oscillations in its

core, but does not break up. It was also difficult to obtain a significant number of velocity measurements because tracer particles did not migrate there in large enough numbers. However, the measurements shown in Fig. 13 demonstrate a core structure that is similar to the larger vortex. The fact that this vortex does not break up may be an indication of the stabilizing effect of the intake jet on this vortex.

The following deductions can now be made: 1) The flow structure exhibits an inviscid instability that can be scaled by the parameter K. 2) The dimensionless vorticity distribution is unaffected by valve lift or stroke length until the occurrence of breakup. 3) Instability analysis agrees well with the existing theory for unbounded toroidal vortices.

In the next two sections the effect of changing the geometry of the cylinder was studied. It was found that, although small changes could have a significant effect on the flow field, the basic characteristics of the flow structure were the same.

C) Effect of valve angle - In tests 6 and 7 the valve seat angle, as defined by S.A. in Fig. 2, was changed. The pictures in Figs. 20a and 20b indicate that for high valve lifts (left and center

columns), the flow field is essentially unaffected by the seat angle. However, seat angle becomes important for case 7b, where S.A. = 30° and the lift is small (L = .07). Under these conditions (Figs. 20a and 20b, right column), the intake jet becomes bistable; i.e., at times, it adheres to the cylinder head while sometimes it remains detached. In the cases where the jet was attached to the cylinder head, it was found that the flow structure of the lower vortex became unstable prematurely while no upper vortex was formed. This seems to be a further indication that the intake jet had a stabilizing effect on the vortices in the previous cases, because when its direction is changed, the vortex becomes more unstable.

D) Effect of valve offset - Since conventional engines do not have axisymmetrically located intake valves, the model was also operated with an off-center valve to study the effect of that change in geometry. Figures 21a and 21b indicate that in this case the vortex is again present, at least for part of the stroke. However, the planes of the axes of rotation of the vortices are no longer perpendicular to the cylinder axis but are tipped at an angle to it. Also, with this change in geometry, the lifetime of the vortex is shorter as in the case of the

shallower valve angle.

It should be noted also that results obtained by Willis[24] seem to indicate that the ring vortex type structures are present even in the significantly more complicated flow field of the shrouded offset intake valve. It also becomes clear that, if the geometry of the model is altered, new parameters are introduced which have to be considered for their effect on the flow structure.

E) Particle trajectories - By operating the movie camera at high enough speeds, the images of the tracer particles were captured on film without blurring. Consequently, it was possible to follow a single pellet for a signficant number of crank angles.

Figure 22 shows the simultaneous trajectories of five different particles that were obtained in this fashion for the axisymmetric case. The letters A through E represent the location of each particle and the piston face at a given crank angle. Each line represents the path of one particle. This figure indicates that the assumption, that the flow with the centrally located intake valve is axisymmetric, is accurate. Also, it is observed that the particles do not frequently enter and leave the .25 in. lighted zone or cross each other's paths.

This has to be the case if the streak method is to be relied upon to produce accurate velocity measurements.

F) Concluding remarks - Under certain conditions where the lower vortex did not break up, a significant portion of the mean flow kinetic energy that entered the cylinder through the intake valve was found to be conserved in the lower vortex. In the cases where the vortex structure was destroyed, a rapid loss of kinetic energy was observed in the mean flow. This implies that if the vortex breaks up late in the compression stroke, the stored kinetic energy of the ring vortex can significantly affect the levels of turbulence intensity long after induction is over. In certain cases in this experiment, the lower vortex was observed to break up as much as 70 crank angle degrees after the BDC of the induction stroke.

VI. Conclusions

Flow visualization has made it possible to observe the flow field during induction as a whole instead of concentrating on one single point in the cylinder volume. It has been possible to isolate the important characteristics, such as structure and stability, by concentrating on a simplified geometry.

Results obtained here can be extended qualitatively to actual engines. The vortex ring structure, if present in an actual engine cylinder, could upon breakup increase combustion rates by increasing turbulence levels in the cylinder prior to ignition. A bistable intake jet could cause large cycle-to-cycle variations. Ring vortices could enhance charge stratification in stratified charge engines by isolating pockets of incoming mixture. Small design changes from engine to engine can have a significant effect on engine behavior.

However, the following conclusions can be applied with confidence only to the model in question and must await more extensive hot-wire or LDV checks in actual engines to ascertain their importance.

1) Under most conditions, the flow field was structured throughout the entire intake stroke. This structure,

when present, was independent of Reynolds number for the range of RPM studied.

2) Small changes in geometry could significantly affect the flow field.

3) For the axisymmetric case: a) The vortex development, diameter and location, scale with piston displacement; b) Velocities in the vortices scale with flow velocities at the valve; c) Vortex breakup is due to an inviscid instability that scales with K and is independent of Reynolds number.

4) Ring vortices, when intact, can conserve significant amounts of the incoming kinetic energy of the flow.

5) When the toroidal vortices are present, the flow is highly repeatable.

6) Ring vortices are also present in off-center valve geometry.

7) Stability analysis agrees with existing theory developed for unbounded ring vortices.

REFERENCES

1. R.K. Bartan et al., "An Empirical Model for Correlating Cycle-by-Cycle Cylinder Gas Motion and Combustion Variations of a Spark Ignition Engine." Paper 710163 presented at SAE Automotive Engineering Congress, Detroit, Michigan, January 1971.

2. R.E. Winsor and D.J. Patterson, "Mixture Turbulence - A Key to Cyclic Combustion Variation." Paper 730086, SAE Transactions, 1973.

3. T. Tanuma et al,"Ignition, Combustion and Exhaust Emissions of Lean Mixtures in Automotive Spark Ignition Engines." Paper 710159 presented at SAE Automotive Engineering Congress, Detroit, Michigan, January 1971

4. R.J. Tabaczynski, "Turbulence and Turbulent Combustion in Spark-Ignition Engines." Prog. Energy Combust. Sci., vol. 2 (1976), pp. 143-165.

5. N.C. Blizard and J.C. Keck, "Experimental and Theoretical Investigation of Turbulent Burning Model for Internal Combustion Engines." Paper 740191 presented at SAE Automotive Engineering Congress, Detroit, Michigan, February 1974.

6. E.S. Semenov, "Studies of Turbulent Gas Flow in Piston Engines." Tech. Transl. F-97 NASA, pp. 122-147, 1963.

7. P.O. Witze, "Measurements of the Spatial Distribution and Engine Speed Dependence of Turbulent Air Motion in an I.C. Engine." Paper 770220 presented at SAE International Automotive Engineering Congress and Exposition, Detroit, Michigan, February 1977.

8. D.R. Lancaster, "Effects of Engine Variables on Turbulence in a Spark-Ignition Engine." Paper 760159 presented at SAE Automotive Engineering Congress and Exposition, Detroit, Michigan, February 1976.

9. W.A. Bone and D.T.A. Townend, Flame and Combustion in Gases, London, 1927.

10. D.E. Fuller, "Mixture Motion in an Engine Cylinder." Ph.D. Thesis, March 1975, St. John's College, Cambridge.

11. W.J.D. Annand and G.E. Roe, Gas Flow in the Internal Combustion Engine, Haessner Publishing, Newfoundland, N.J., 1974, pp. 53-75.

12. K.Tanaka, "Airflow Through Exhaust Valve of Conical Seat." Proc. 3rd. Int. Cong. for App. Mechs. 1, pp. 287-295.

13. M. Allen and A. J. Yerman, "Neutral Density Beads for Flow Visualization," Symposium on Flow Visualization, ASME Annual Meeting, November, 1960.

14. E.C. Roberson, "The Development of a Flow Visualization Technique." Report of the National Gas Turbine Establishment, No. R. 181, Pyestock, Hants., November 1955.

15. F. Odar and W.S. Hamilton, "Forces on a Sphere Accelerating in a Viscous Fluid." J. Fluid Mech., vol. 18 (1964), pp. 302-314.

16. J. Faure, "Quelques limitations theoriques des procedes de visualization." La Houille Blanche, N°3, May, 1963.

17. T. Maxworthy, "The Strucutre and Stability of Vortex Rings." J. Fluid Mech., vol. 51, part 1 (1972), pp. 15-32.

18. T. Maxworthy, "Some Experimental Studies of Vortex Rings." J. Fluid Mech., vol. 81, Part 3 (1977), pp. 465-495.

19. J.P. Sullivan, S.E. Widnall and S. Ezekiel, "Study of Vortex Rings Using a Lazar Doppler Velocimeter," AIAA Journal, vol. 11, No. 10, October, 1973.

20. S.E. Widnall, D.B. Bliss and C-Y. Tsai, "Instability of Short Waves on a Vortex Ring." J. Fluid Mech., vol. 66 (1974), pp. 35-48.

21. C-Y Tsai and S.E. Widnall, "The Stability of Short Waves on a Straight Vortex Filament in a Weak Externally Imposed Strain Field." J. Fluid Mech., vol. 73, part 4 (1976), pp. 721-733.

22. P.G. Saffman, "The Number of Waves on Unstable Vortex Rings," J. Fluid Mech., vol 84, part 4 (1978), pp. 625-639.

23. W.B. Wallace, "High-Output Medium-Speed Diesel Engine Air and Exhaust System Flow Losses," Proc. Instu. Mech. Engrs., 1967-68, vol. 182, part 3D.

24. D.A. Willis, W.E. Mayer and C. Birnie, Jr., "Mapping of Airflow Patterns in Engines with Induction Swirls." Paper 66093 presented at SAE Automotive Engineering Congress, Detroit, Michigan, January 1966.

25. A.P. Morse, J.H. Whitelaw and M. Yianneskis, "Turbulent Flow Measurements by Laser-Doppler Anemometry in a Motored Reciprocating Engine." Imperial College, London, unpublished.

26. P.A. Thompson, Compressible-Fluid Dynamics, McGraw-Hill, New York, 1972, pp. 137-143.

27. S.K. Karanfilian and T.J. Kotas, "Drag on a Sphere in Unsteady Motion in a Liquid at Rest." J. Fluid Mech., vol. 87, part 1 (1978), pp. 85-96.

APPENDIX A - SCALING OF THE WATER MODEL TO ENGINE INTAKE CONDITIONS

During the intake process of an internal combustion engine, air is commonly assumed to be an incompressible fluid. A criterion for compressibility can be obtained from the continuity equation:

$$\vec{\nabla} \cdot \rho\vec{V} + \frac{\partial \rho}{\partial t} = 0 \qquad [A\text{-}1]$$

This can be written in a different form by expanding the first term on the left-hand side and using the definition of the substantial derivative $\frac{D()}{Dt} = u \cdot () + \frac{\partial()}{\partial t}$

$$\vec{\nabla} \cdot \rho\vec{V} + \frac{\partial \rho}{\partial t} = \rho\vec{\nabla}\cdot\vec{V} + \vec{V}\cdot(\vec{\nabla}\rho) + \frac{\partial \rho}{\partial t}$$
$$= \rho\vec{\nabla}\cdot\vec{V} + \frac{D\rho}{Dt}$$

So, after simplifying further,

$$-\frac{1}{\rho}\frac{D\rho}{Dt} = \vec{\nabla}\cdot\vec{V} \qquad [A\text{-}2]$$

Consequently, $\vec{\nabla}\cdot V$ is a measure of the change in density in the flow field; and the fluid may be assumed to be incompressible if the nondimensional form of this quantity is significantly smaller than 1.

$$\vec{\nabla}^* \cdot V^* << 1 \qquad [A\text{-}3]$$

where

$$\vec{\nabla}^* = D_p\vec{\nabla}$$

$$\vec{V}^* = \frac{\vec{V}}{\bar{V}_p}$$

For an excellent discussion of the effect of compressibility see Thompson.[26] The commonly accepted limit where compressibility can be neglected is where Mach numbers are below 0.3, such that

$$\vec{V}^* \cdot \vec{V}^* \approx .1$$

is small.

The nondimensional form of the momentum equation where the fluid can be assumed incompressible is:

$$[St]\ \frac{\partial \vec{V}^*}{\partial t^*} + (\vec{V}^* \cdot \vec{\nabla}^*)\vec{V}^* = -\vec{\nabla}^* P^* + [Re^{-1}]\nabla^{*2}\ \vec{V}^* \qquad [A-4]$$

In this equation the starred quantities are dimensionless variables defined by:

$$\nabla^{*2} = D_p^2\ \nabla^2$$
$$t^* = t\omega$$
$$P^* = \frac{P + \rho g z - P_o}{\rho V_p^2}$$

where 'z' is the vertical coordinate. Because of the absence of a free surface or density gradients in this experiment the gravity term has no effect on the flow and has been absorbed into the pressure term. P_o is a typical ambient pressure.

Two parameters, Reynolds number

$$Re = \frac{\bar{V}_p D_p}{\nu}$$

and Strouhal number

$$St = \frac{\omega D_p}{\bar{V}_p}$$

appear in Eq. A-4 and must be matched in the model with actual engine conditions. However, since engine shaft speed is directly proportional to the characteristic velocity $\bar{V}_p$ that is observed in the cylinder,

$$\bar{V}_p \sim \omega S$$

geometric similitude automatically leads to a Strouhal number match.

Matching Reynolds numbers between experiment and actual engine operating conditions

$$\left(\frac{\bar{V}_p D_p}{\nu}\right)_{\text{model}} = \left(\frac{\bar{V}_p D_p}{\nu}\right)_{\text{engine}}$$

while observing the geometric restriction leads to

$$\frac{\bar{V}_{p\ \text{model}}}{\bar{V}_{p\ \text{engine}}} = \frac{\nu\ \text{air}}{\nu\ \text{water}}$$

For the conditions of this experiment this ratio was 1:17.

APPENDIX B - RESPONSE TIME OF POLYSTYRENE PARTICLES OF TYPICAL DIAMETER

The response time of a typical polystyrene pellet, .03 inches in diameter, to a step change in velocity of 15 inches per second was calculated. This velocity was characteristic of the velocities that were encountered in the cylinder in this experiment.

Because of the unsteady nature of the motion of the polystyrene pellets under these conditions, the effect of the 'virtual mass' and the history of the motion had to be considered.[15] The pellet was assumed to be spherical in shape and the drag force on it was calculated by using

$$-F_D = \frac{1}{8}C_V\pi\delta^2\rho|V|V + \frac{1}{6}C_A\pi\delta^3\rho\dot{V} + \frac{1}{4}C_H\delta^2(\pi\rho\mu)^{\frac{1}{2}}\int_o^t \frac{\dot{V}(t')}{(t-t')^{1/2}}dt' \qquad [B-1]$$

where

F_D = drag force

δ = particle diameter

ρ = fluid density

μ = fluid viscosity

V = particle velocity relative to fluid

$\dot{V}$ = particle acceleration relative to fluid

C_V = steady state drag coefficient

C_A = virtual mass coefficent

C_H = flow history coefficent

The form of the expression was determined by Boussinesq in 1885 in a theoretical calculation where he neglected the convective terms in the momentum equation. The values of the coefficients, C_A and C_H, used in this calculation were obtained from the experimental study of the drag force on a sphere in sinusoidal motion.[15] The value of the steady state coefficient was determined from the expression given by Karanfilian and Kotas.[27]

In calculating the response time of the pellet, it was assumed that drag on the particle was the only force acting on it and Eq. B-1 was integrated numerically to obtain the velocity of the pellet as a function of time. It was found that the particle increased in speed from 10 percent to 90 percent of the fluid velocity 16 milliseconds after the step change.

Using the same equations it was found that the velocity of the polystyrene pellets that was induced by gravity was an order of magnitude lower than characteristic flow velocities. Also, the total distance traveled by these pellets due solely to the effect of gravity in the time scale of the longest experiment was ~.2 inches. Consequently, the effect of gravity on the particle is negligible.

APPENDIX C - CALCULATION OF THE KINETIC ENERGY OF THE VORTICES

For the purpose of this calculation, the velocity distribution in the vortex was assumed to be given by the Ω vs. R curves, such as Fig. 11, except in the region of the axis of rotation of the vortex. Eq. [1] can not be used for R = 0 since at that point the velocity would become infinite. A solid body rotation was assumed up to R = .07 since it was observed from the data that the velocity was an increasing function (with decreasing R) up to this point.

With these assumptions, the energy in each vortex was calculated from

$$(K.E.)_{vortex} = \pi^2 D_v \rho \int_o^r r[V(r)]^2 \, dr \qquad [C-1]$$

where V and r are the dimensional velocity distribution and radial position in the vortex. The value of r' in the equation was determined from photographs. When the cross section of the vortex was not circular an average of the maximum and the minimum value of the radius was used.

The total kinetic energy flux of the mean flow was also calculated from

$$(K.E.)_{inducted} = \frac{1}{2} \frac{\rho A_e}{\omega} \int_o^{\pi} [V'(\theta)]^3 d\theta \qquad [C-2]$$

where V' and A_e are the mean flow velocity and the effective flow area of the valve. The effective flow area is equivalent to a fraction (the discharge coefficient C_f) of the actual valve area (πLD_o^2).

It was found that the energy contained in the two toroidal vortices at bottom dead center was a significant fraction of the total kinetic energy flux during induction. This calculation was sensitive to the value of the discharge coefficent. In these experiments values of .6 and .8 were used for C_f and the fraction of energy in the vortices ranged from 30 percent to 56 percent of the total inducted into the cylinder. Consequently, if the vortices are present at BDC they will contain a significant portion of the total kinetic energy. It is, however, difficult to determine an exact fraction because of the dependence on C_f which is an unknown in this case.

It should also be noted that the energy loss due to viscous dissipation in the lower vortex is typically one percent of the total kinetic energy contained in the vortex and can be neglected. Viscous dissipation per unit volume can be determined from

$$e_v = \mu\left[\frac{\partial v_\theta}{\partial r} - \frac{v_\theta}{r}\right]^2$$

where e_v and v_θ are the viscous dissipation per unit volume and tangential velocity in the vortex respectively. In this calculation the assumption must be made that the streamlines are concentric about the axis of rotation of the vortex.

APPENDIX D - CALCULATION OF THE CRITICAL TIME OF BREAKUP AND THE NUMBER OF AZIMUTHAL INSTABILITY WAVES IN THE CORE OF THE VORTEX

It was observed by Maxworthy that after the onset of instability in the core of a ring vortex, the ring traveled downstream approximately five of its initial diameters before breaking up.[18] Consequently, a theoretical time for breakup was defined as

$$t_c' = \frac{5D_o}{U'} \qquad [D-1]$$

where D_o is the initial vortex diameter or the diameter of the generating mechanism and U' is the self-induced velocity of the vortex.

A vortex ring of diameter D_v, in an unbounded fluid, will move with a self-induced velocity of:

$$U = \frac{\Gamma}{2\pi D_v}\left[\ln\left(\frac{8D_v}{d_{ve}}\right) - \frac{1}{4}\right] \qquad [D-2]$$

where Γ and d_{ve} are the circulation around the axis of rotation and the effective diameter of the core of the vortex respectively.[22] The value of d_{ve} is a function of the actual vortex core diameter and the distribution of the vorticity in the core:

$$d_{ve} = d_v e^{\left(\frac{1}{4} - Z\right)} \qquad [D-3]$$

and

$$Z = \frac{4\pi^2}{\Gamma^2} \int_0^{\frac{d_v}{2}} rV^2 dr \qquad [D-4]$$

where r and V are dimensional position and velocity in the core of the vortex, respectively.

From Eq. E-2 and the velocity distribution plots it was possible to calculate a hypothetical velocity U' for this experiment. (The toroidal vortices in the cylinder do not move at this velocity, however, because they are confined). Consequently, a theoretical critical time was obtained from Eq. E-1.

For the typical case of 750 RPM (case 1a) the calculation was conducted for the vortex at the bottom dead center position and a breakup time of .33 seconds was predicted. The time for the stroke was added to this value and Eq. [7] was applied, and this predicted K = 52 for stability. This is in good agreement with the experimental prediction of the critical value of K = 48.

The number of instability waves that were observed by the bubble technique also agree well with a theoretical prediction by Saffman.[22] Using the equation for N, the number of waves

$$N \approx [0.53 + 2.43(D/S)^{2/3}] \left[1 + \frac{0.8}{\epsilon}\right] \qquad [D-5]$$

where ε is defined implicitly in:

$$\varepsilon R^{1/2} = 50\left(\frac{D}{S}\right)^{5/6}\left[1 + 0.22\left(\frac{S}{D}\right)^{2/3}\right]\left[1.24 + \frac{2}{3}\ln\left(\frac{D}{S}\right) + \ln\left[1 + 0.22\left(\frac{S}{D}\right)^{2/3}\right] - \ln(0.47 + .63\varepsilon)\right]^{-1/2} \quad [D\text{-}6]$$

In these equations $\frac{S}{D}$ is the ratio of the length of stroke of the vortex generating mechanism and the diameter of the orifice where the vortex is generated.

From these two equations a value of N = 4 was calculated while three waves were observed for the experimental case.

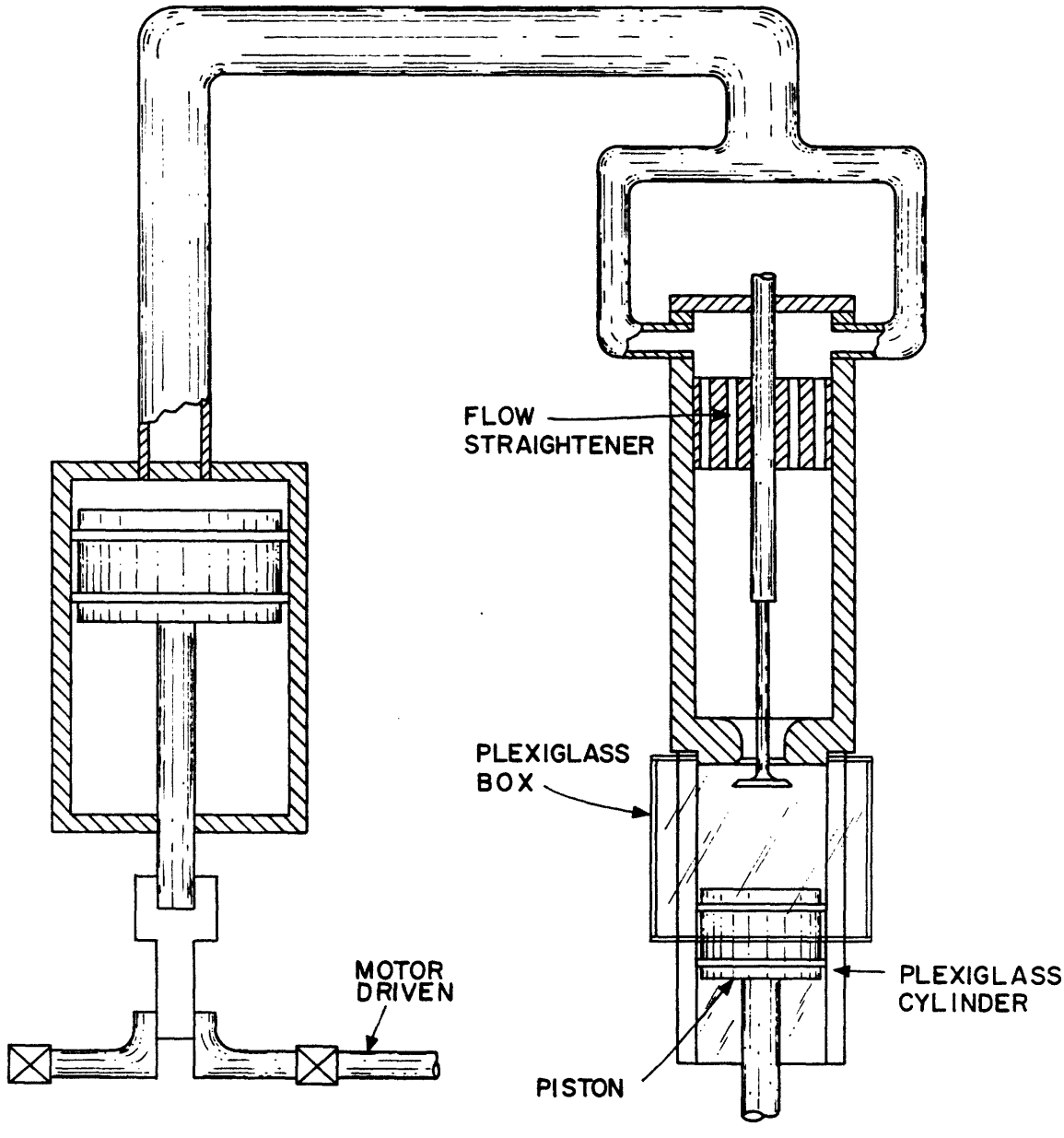

Fig. 1: Schematic of experimental apparatus

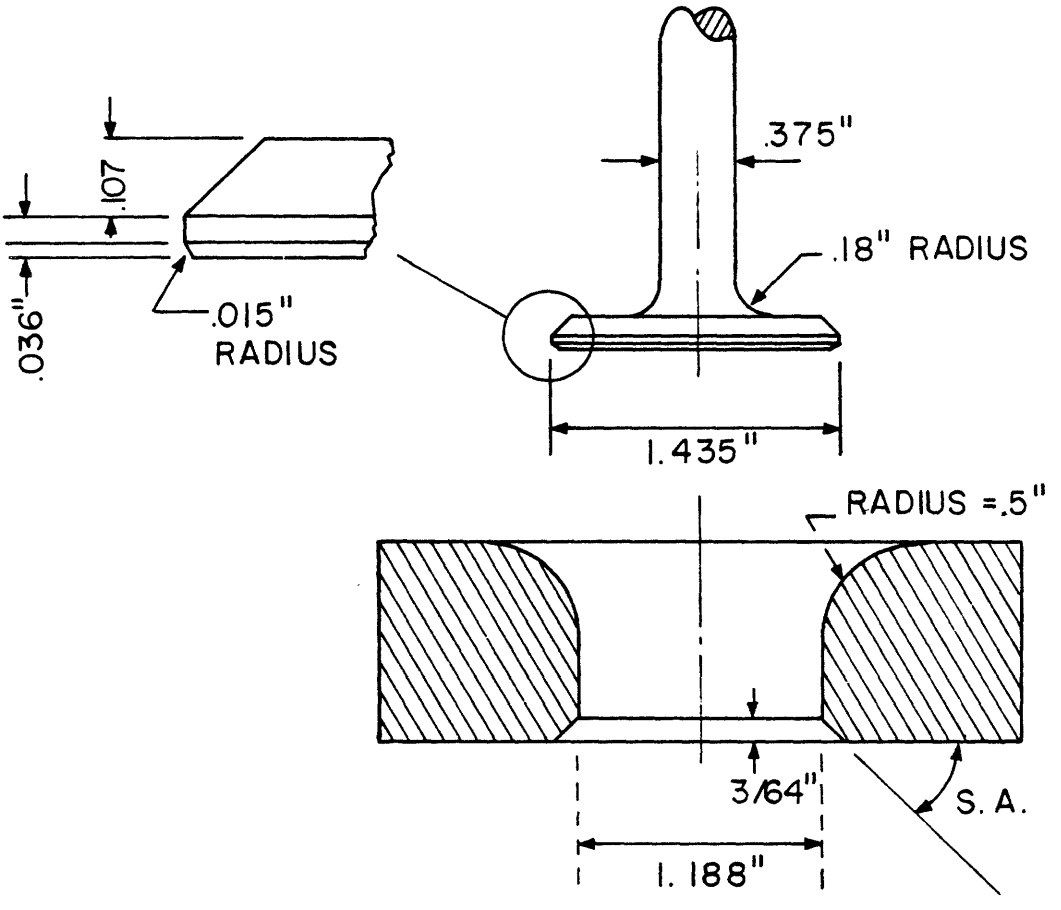

Fig. 2: Intake valve and seat geometry

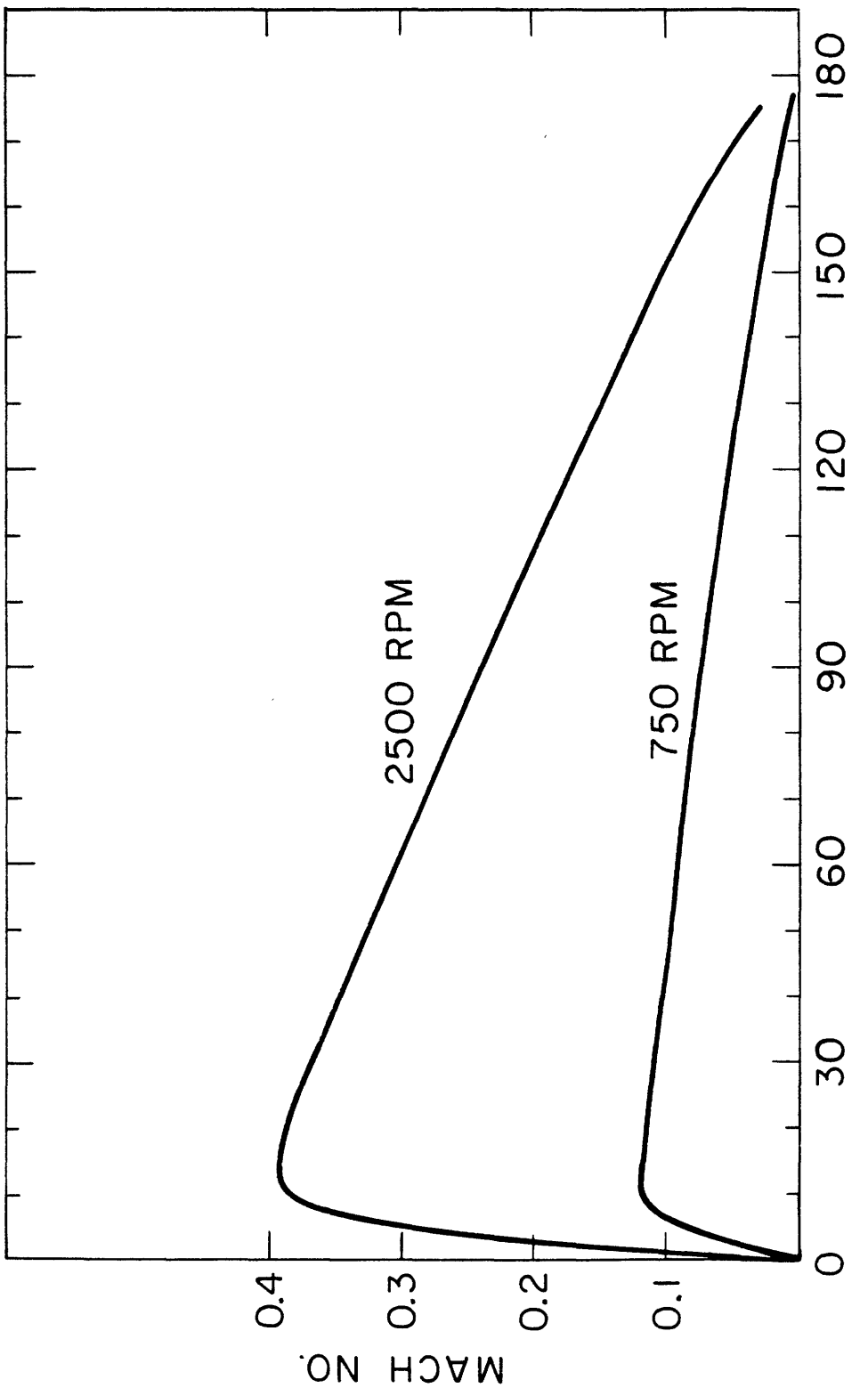

Fig. 3: Mach number at the valve throat during the intake process

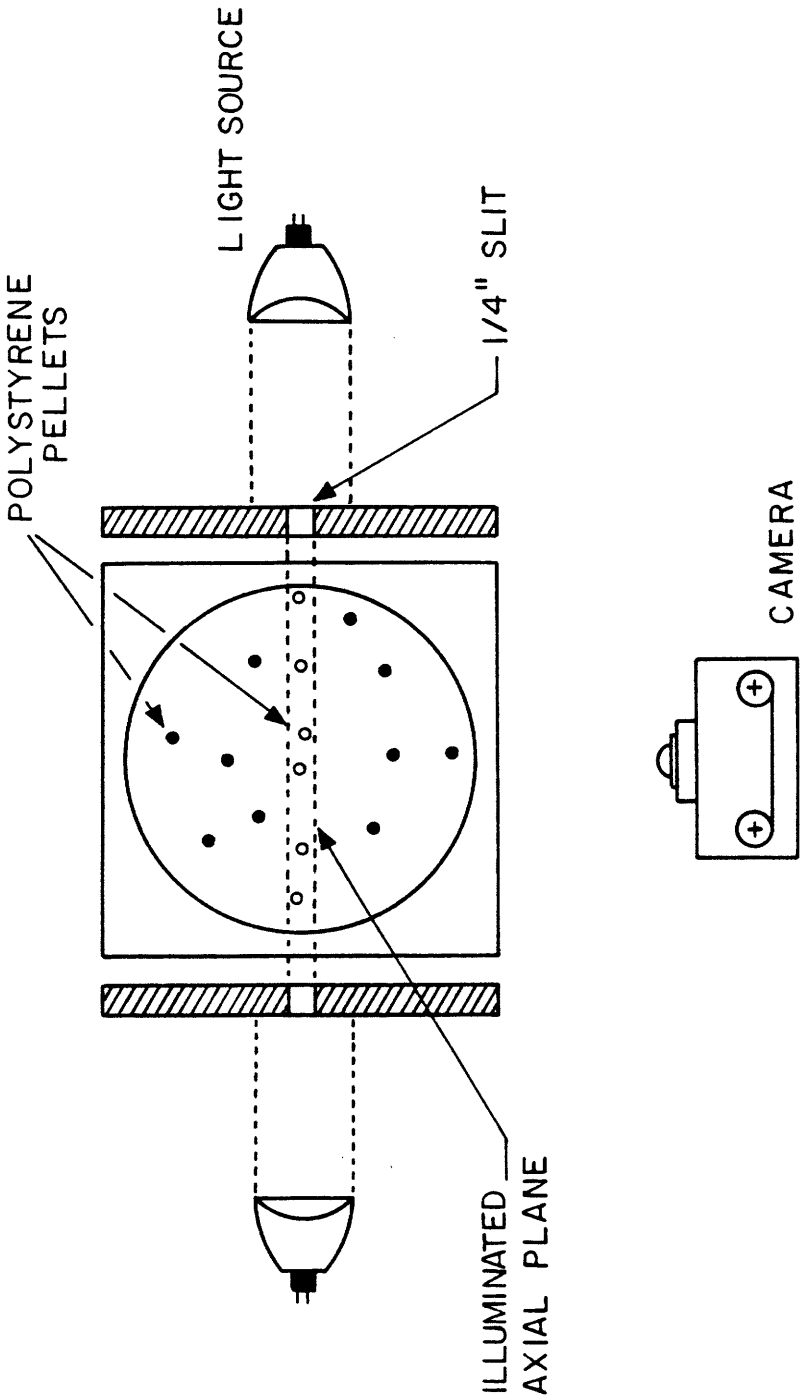

Fig. 4: Photography technique used with polystyrene tracers

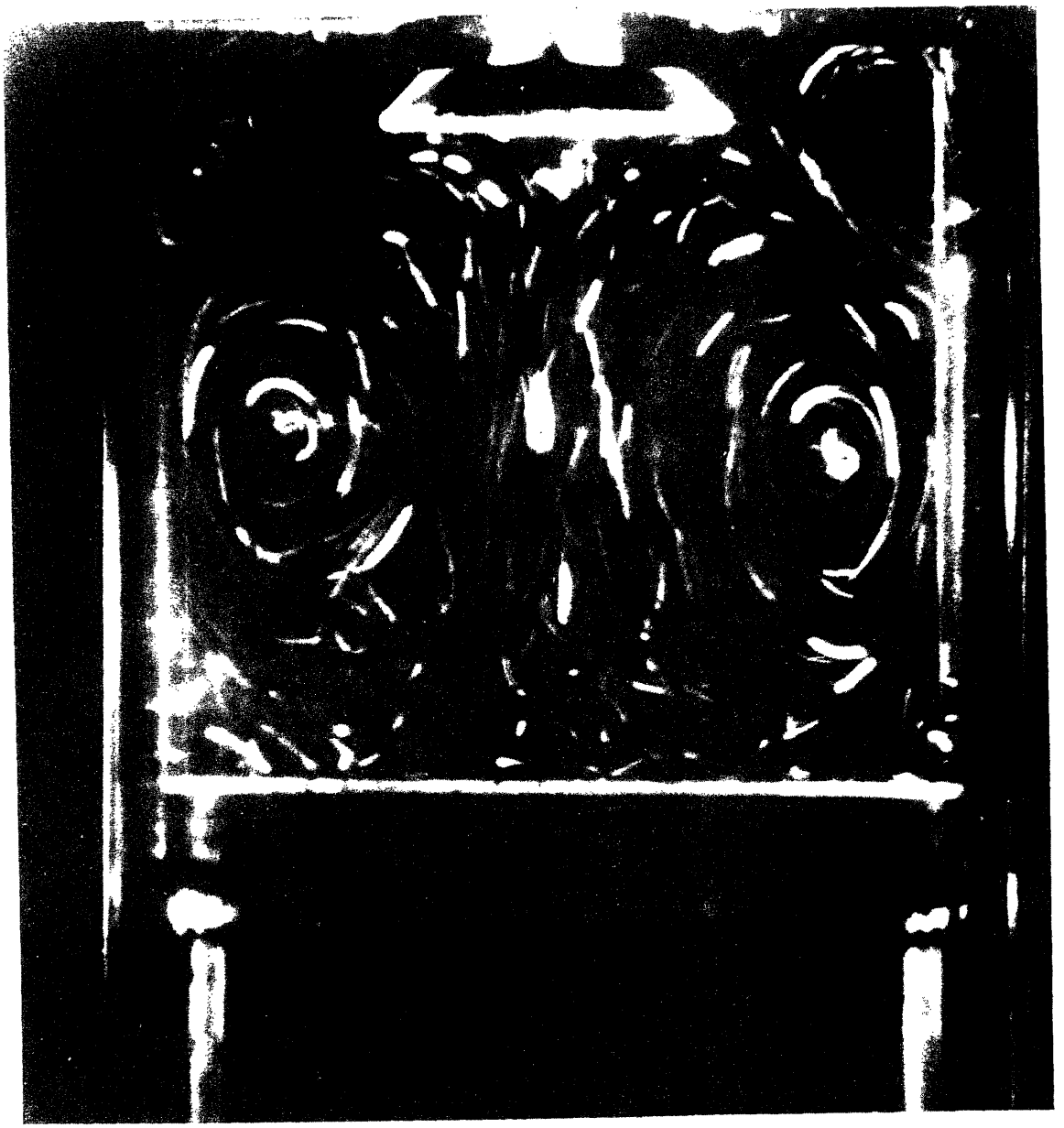

Fig. 5: Typical photograph of the structure of the flow during the intake process

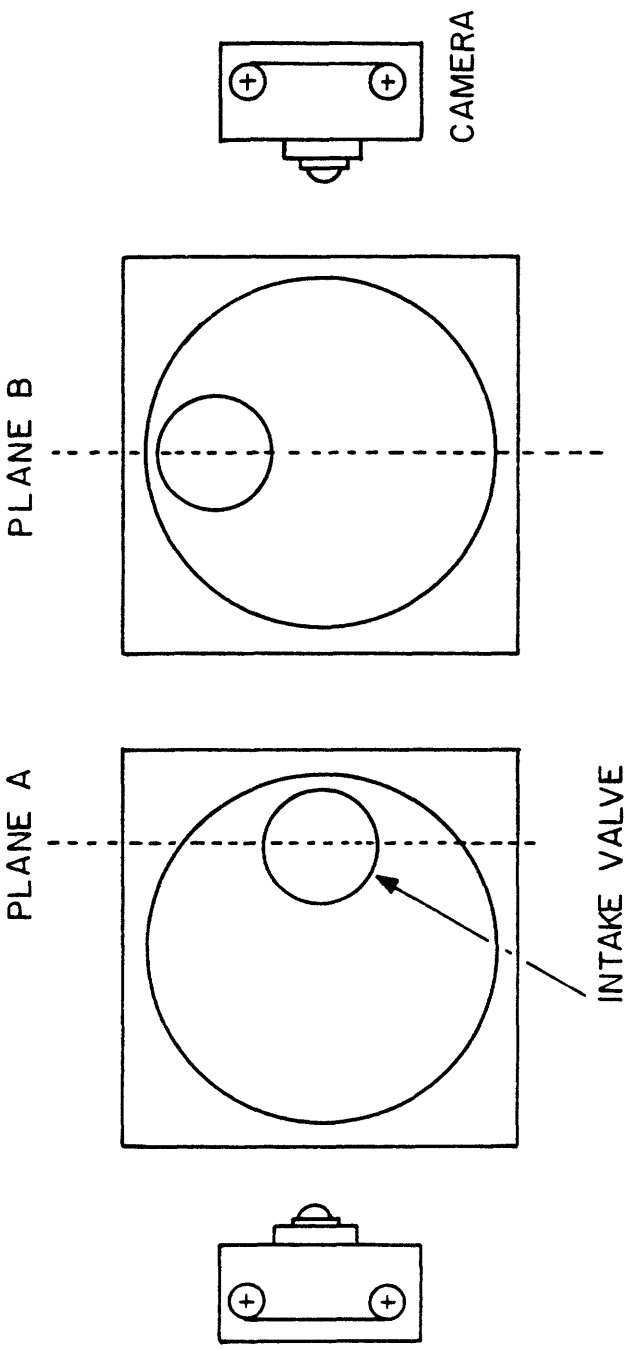

Fig. 6: Planes of the nonaxisymmetric geometry cylinder that were photographed

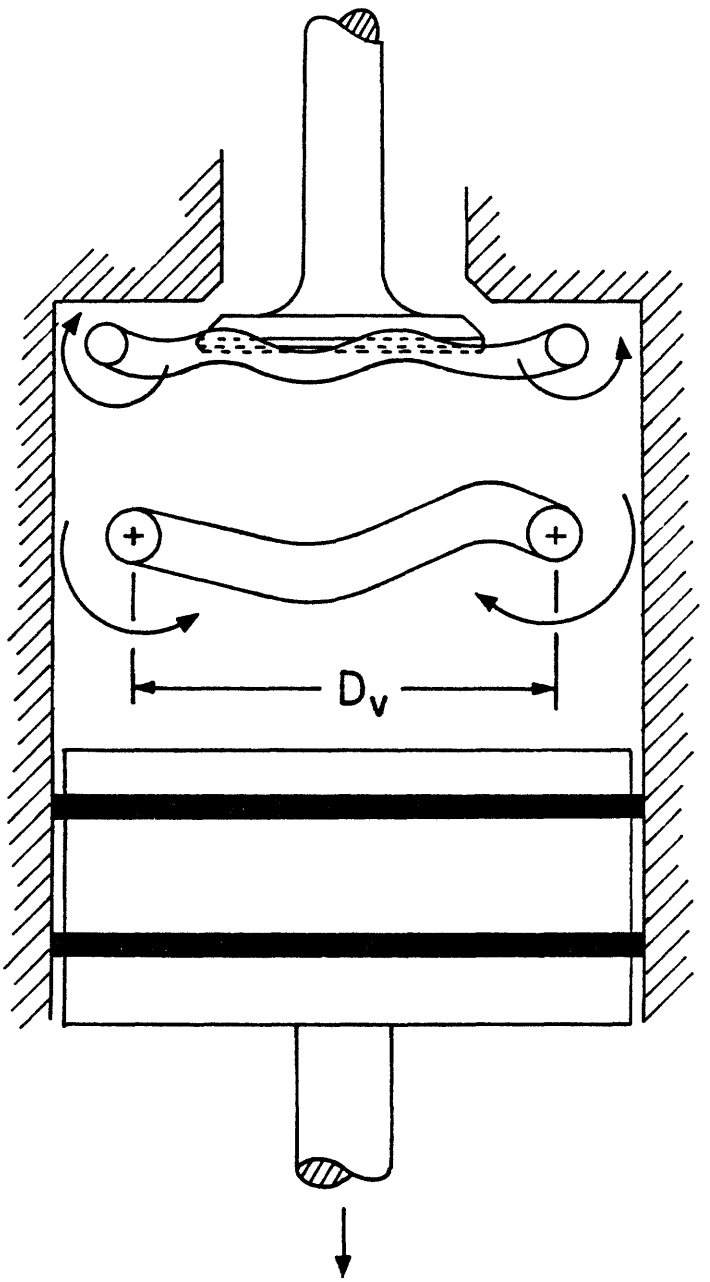

Fig. 7: Positions of the axes of rotation of the two vortices for the axisymmetric case

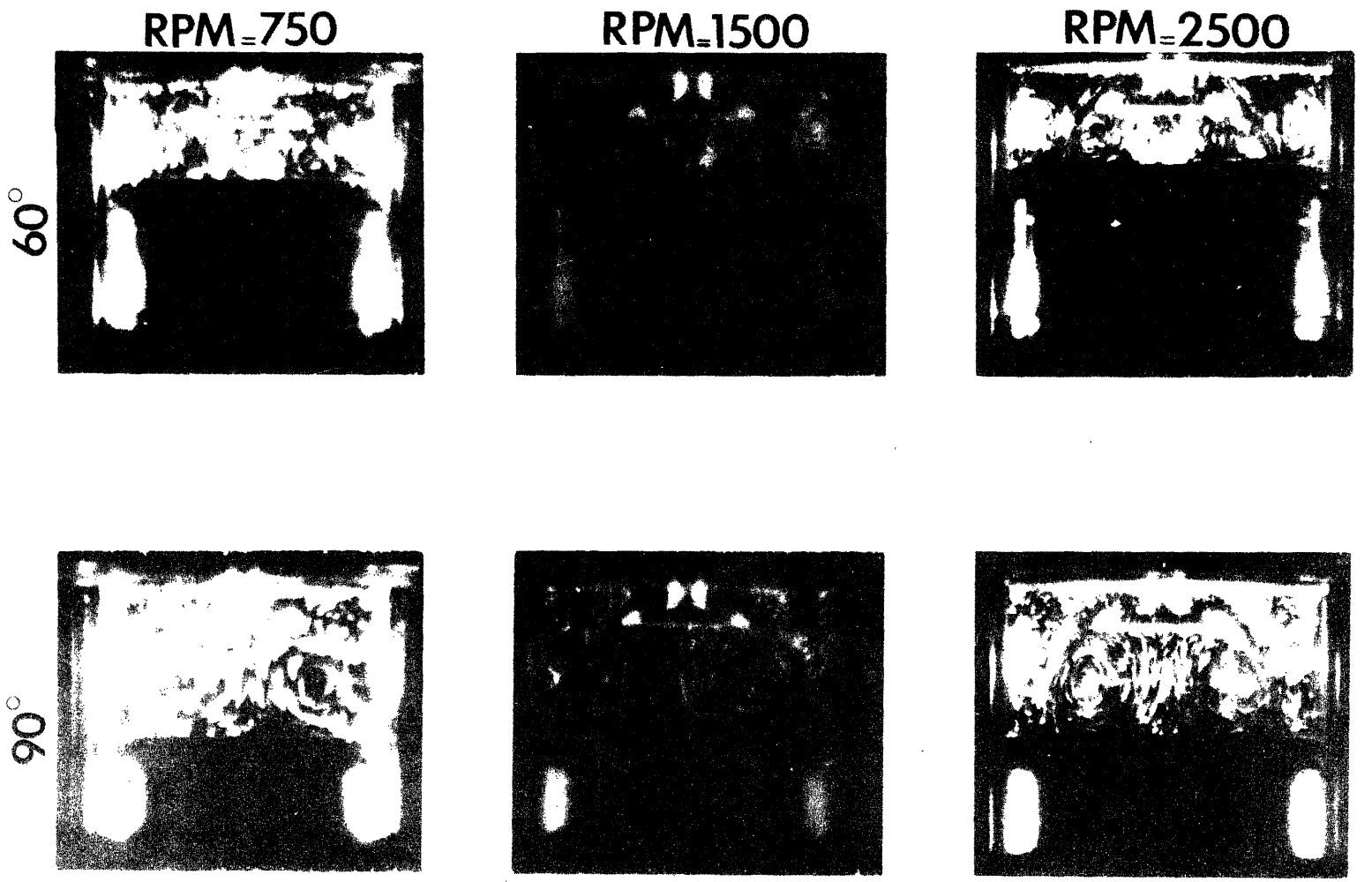

Fig. 8a: Effect of RPM on vortex structure; cases 1a, 2a and 3a

B/S=1.35 LIFT=.21

RPM=750 RPM=1500 RPM=2500

130°

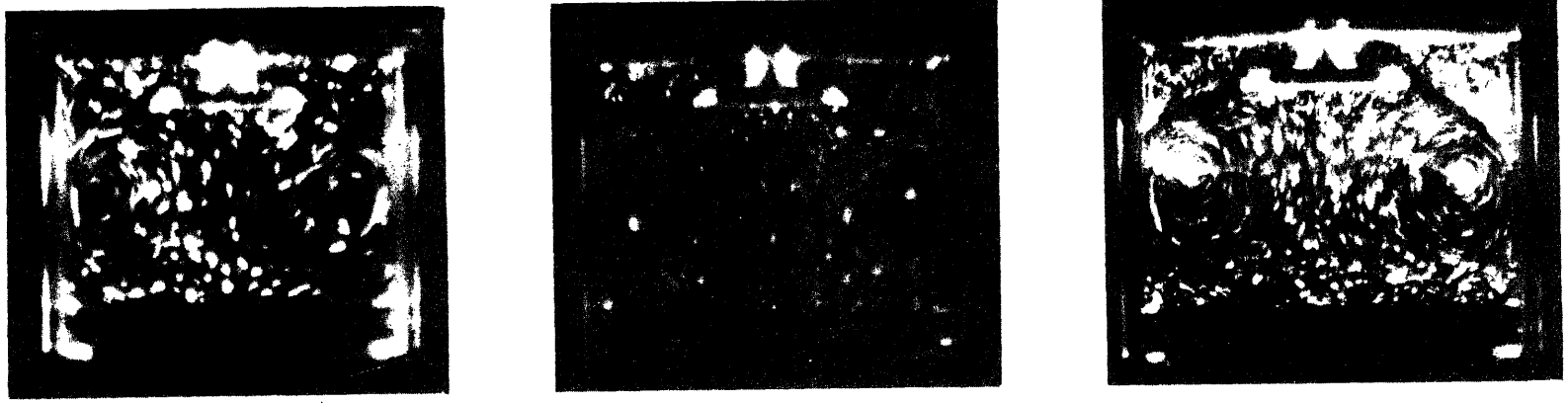

180°

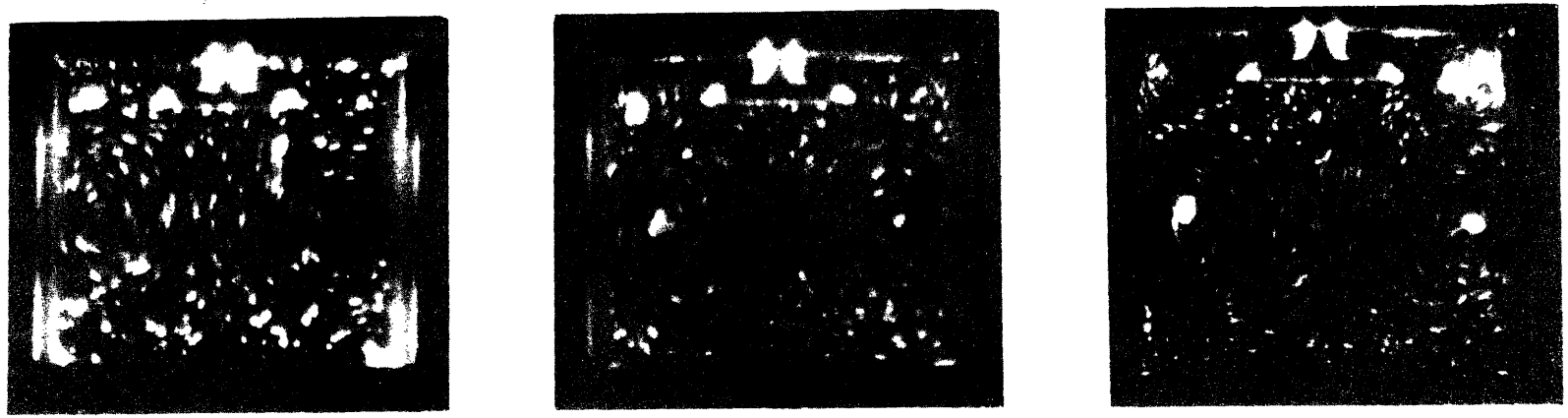

(Fig. 8b)

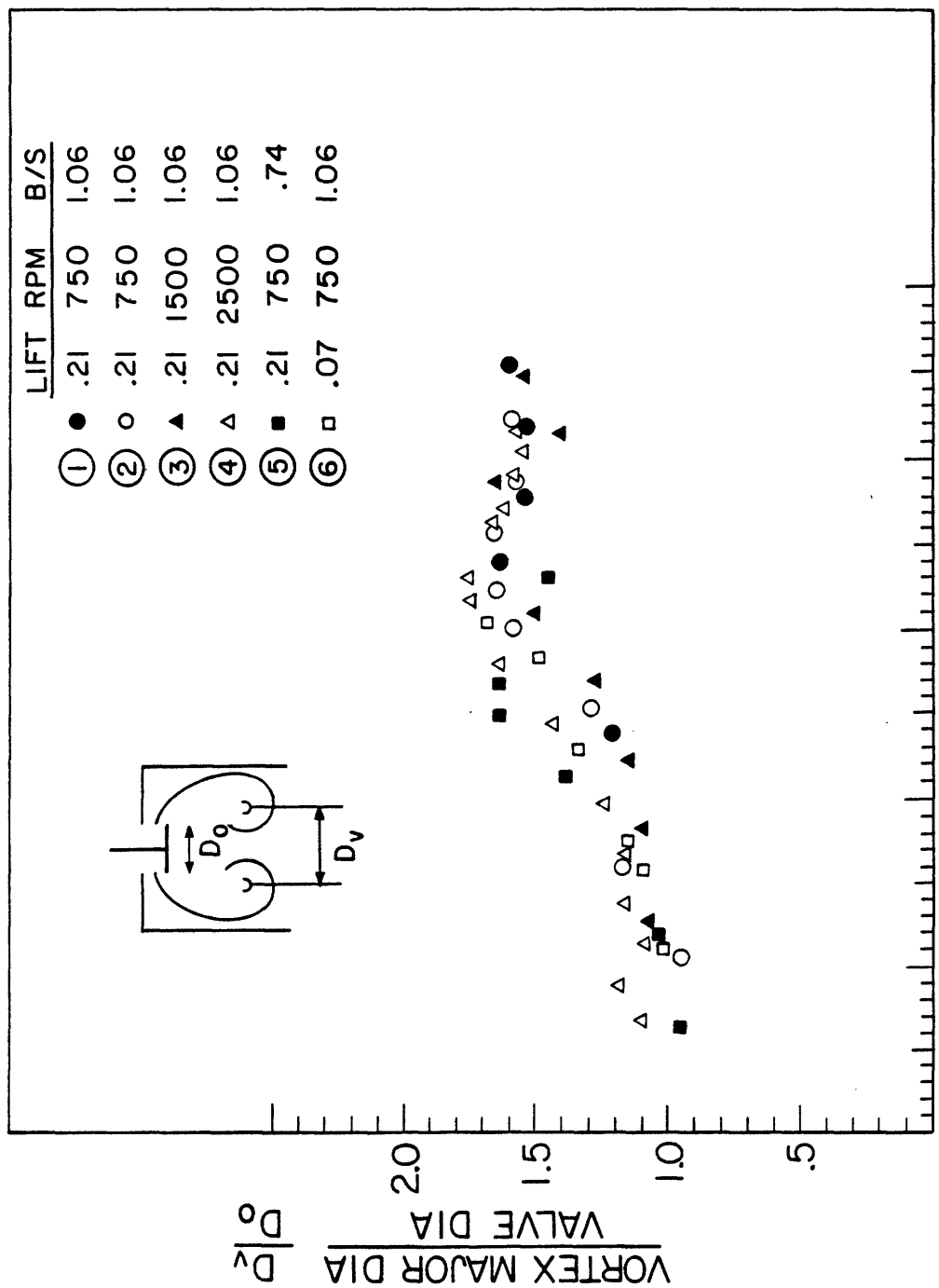

Fig. 9: Variation of dimensionless vortex major diameter with dimensionless displacement

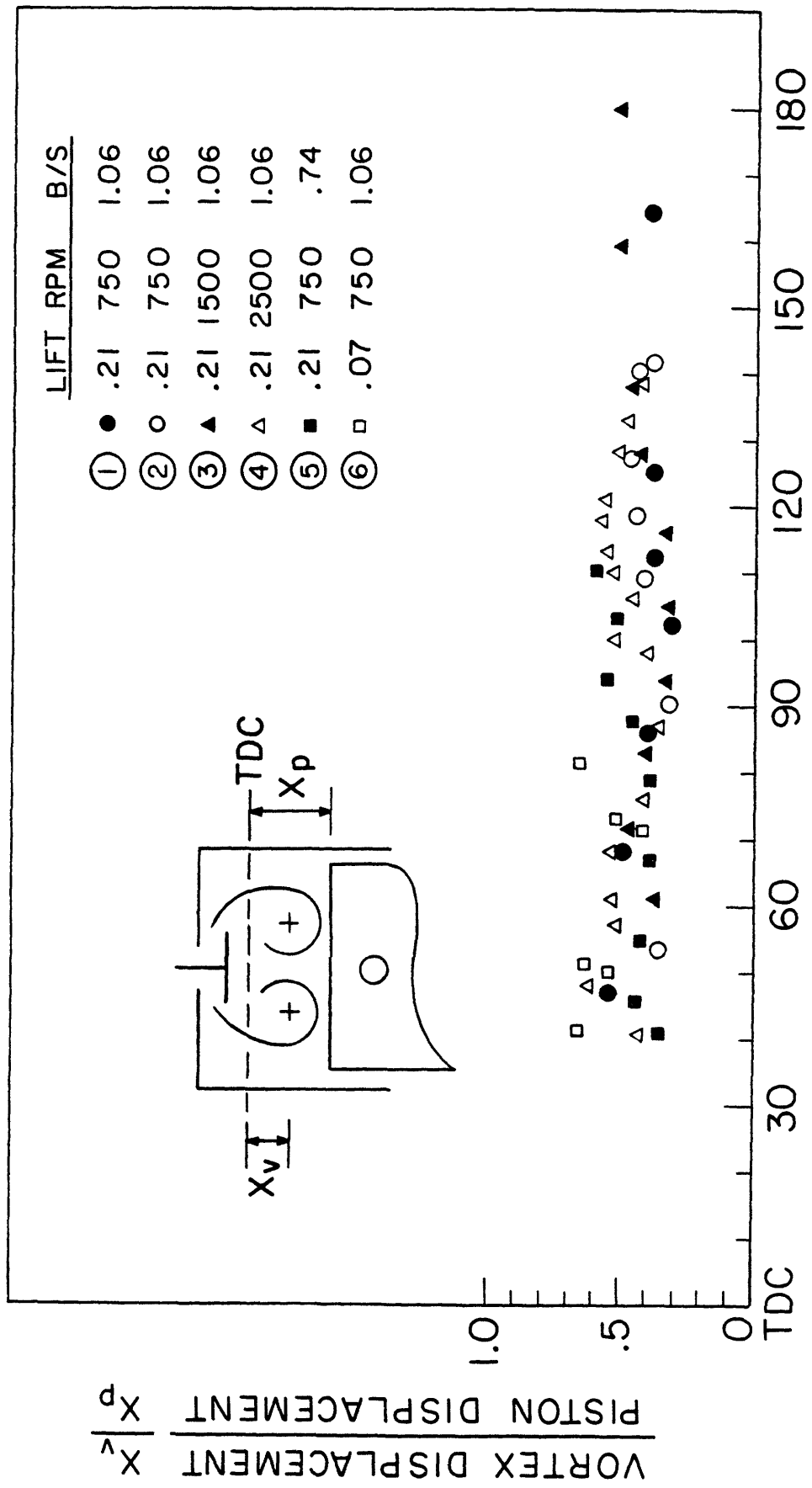

Fig. 10: Variation of vortex nondimensional position with crank angle

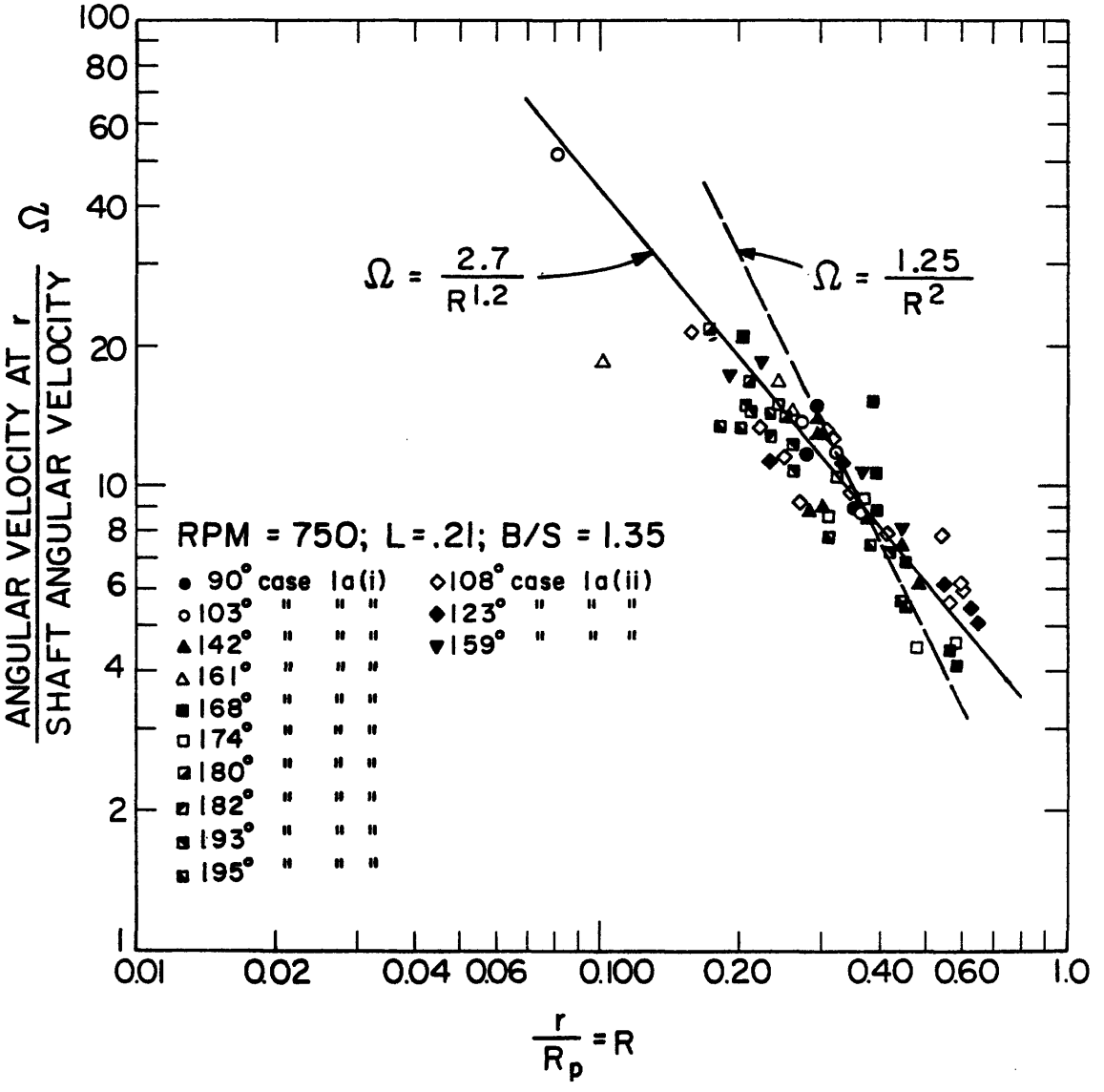

Fig. 11: Variation of nondimensional angular velocity in vortex with nondimensional radius, case Ia

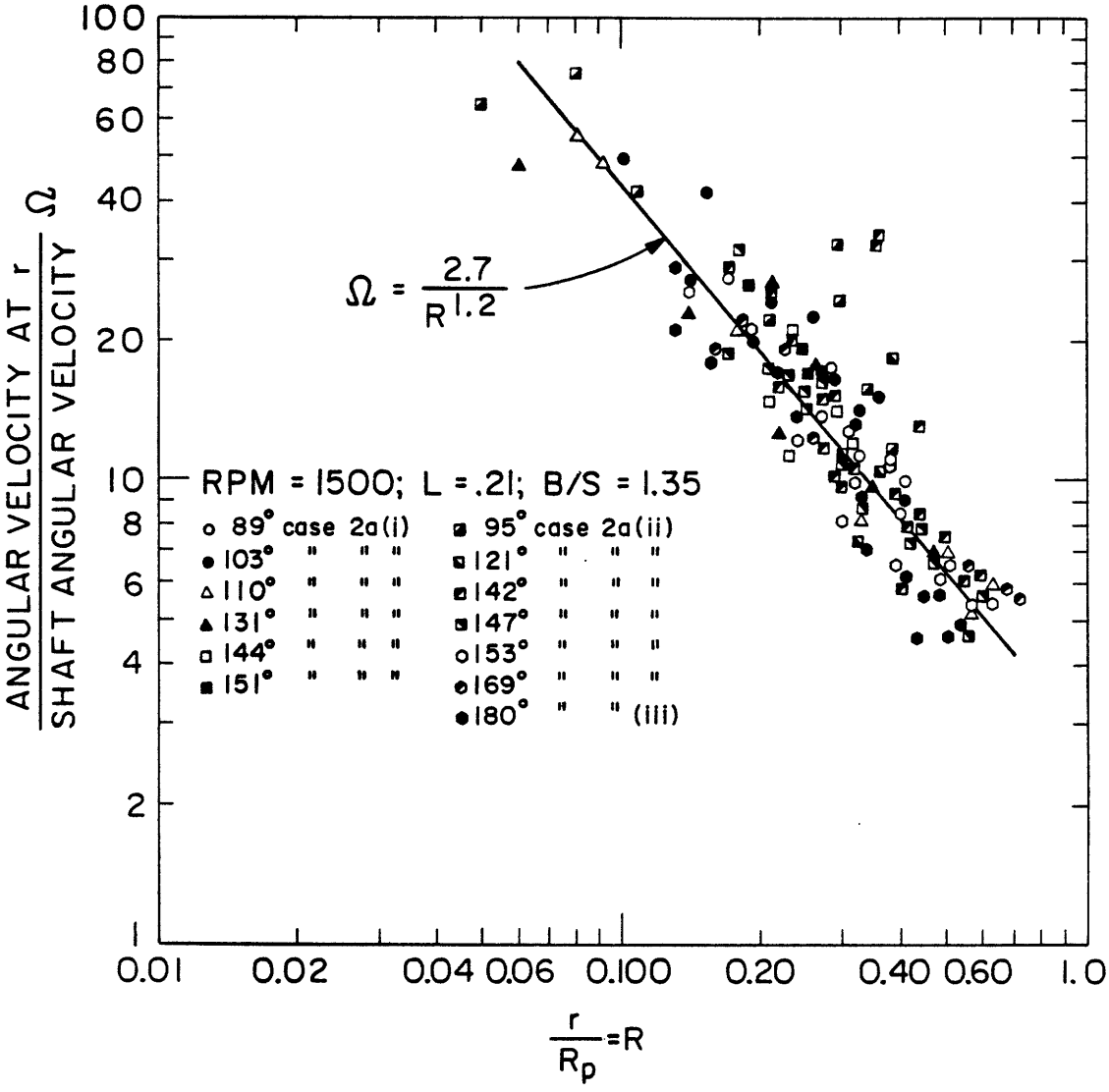

Fig. 12: Variation of nondimensional angular velocity in vortex with nondimensional radius, case 2a

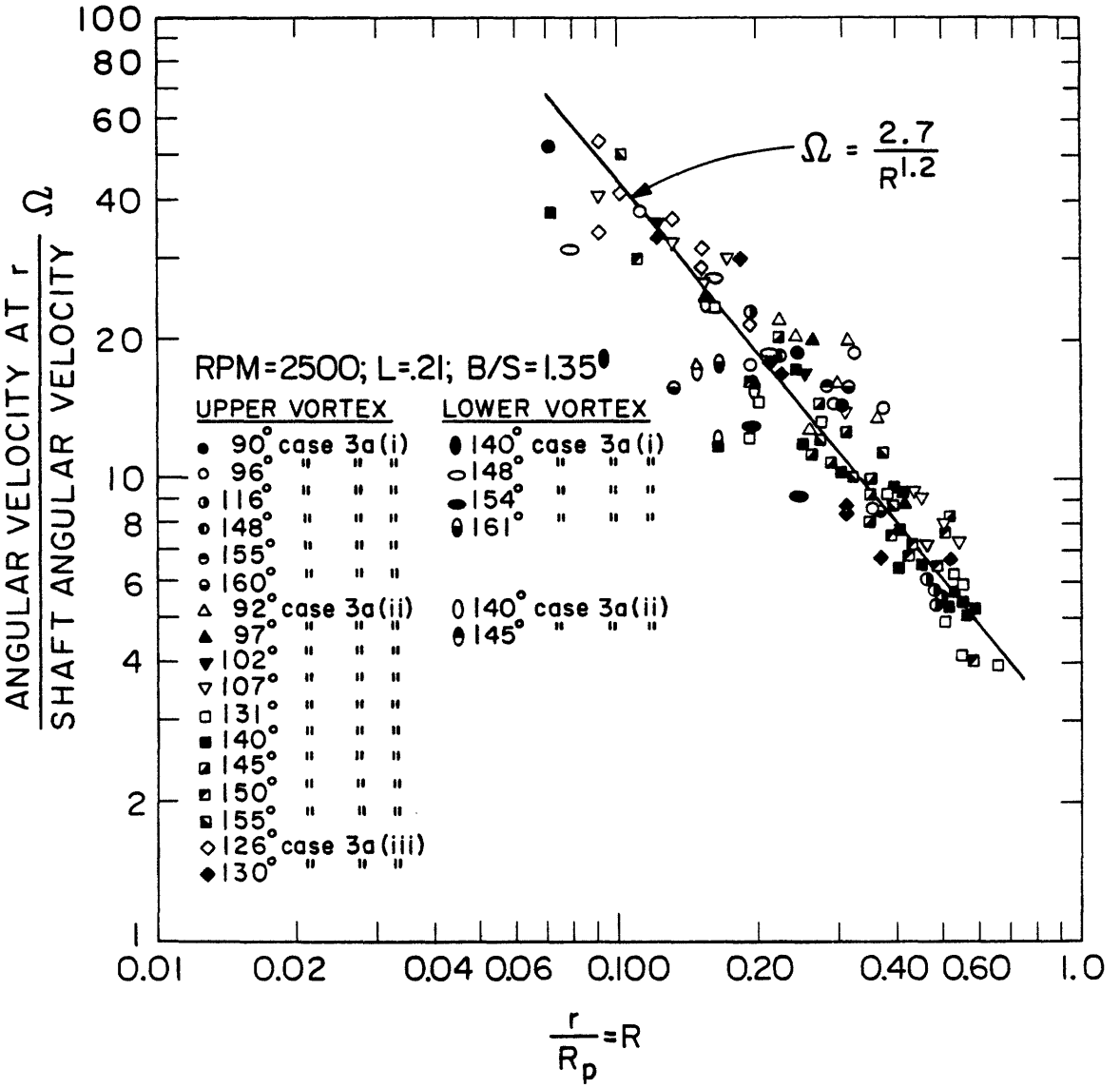

Fig. 13: Variation of nondimensional angular velocity in vortex with nondimensional radius, case 3a

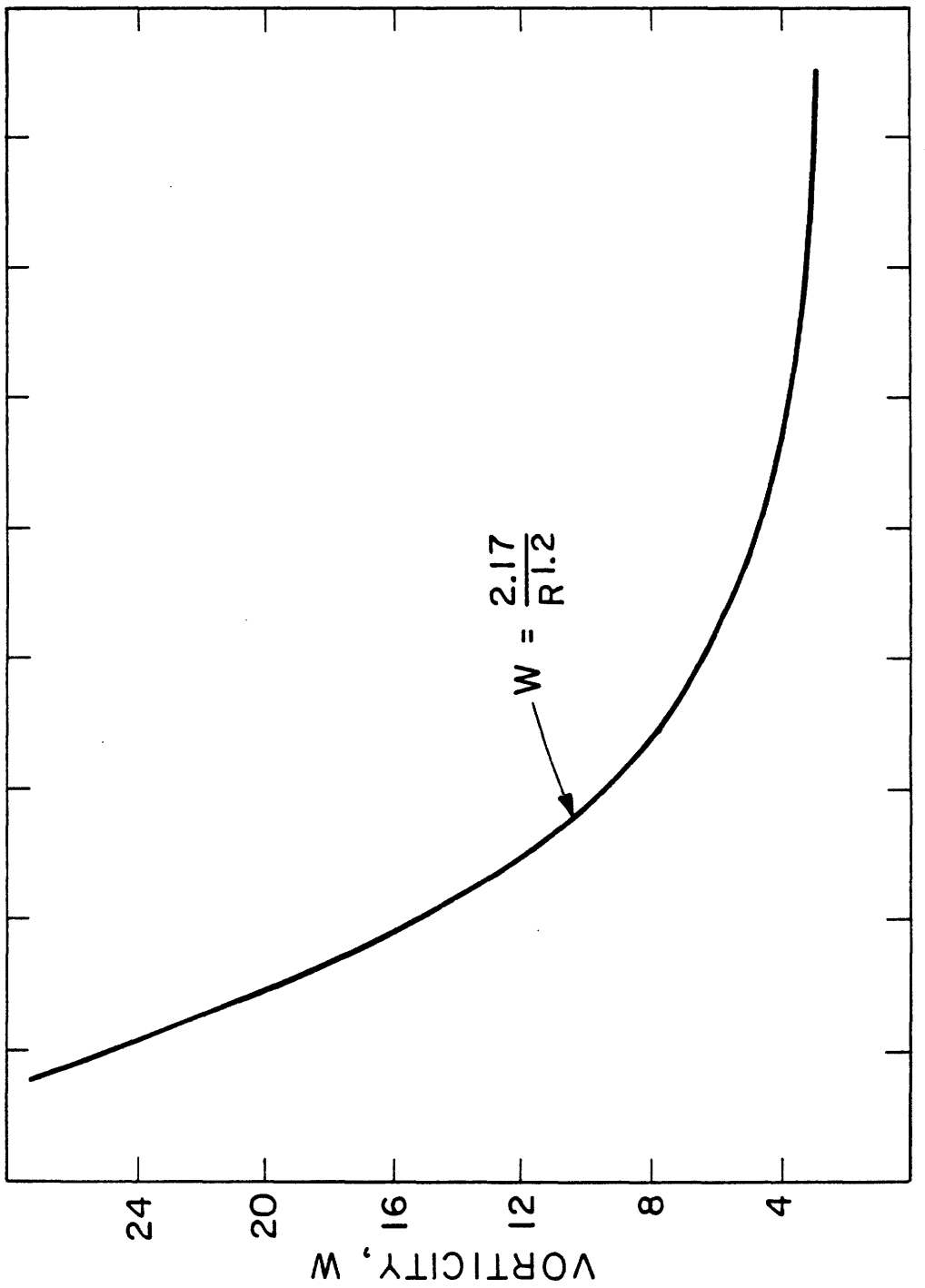

Fig. 14: Variation of nondimensional vorticity, W vs. nondimensional radius, cases 1a, 2a and 3a

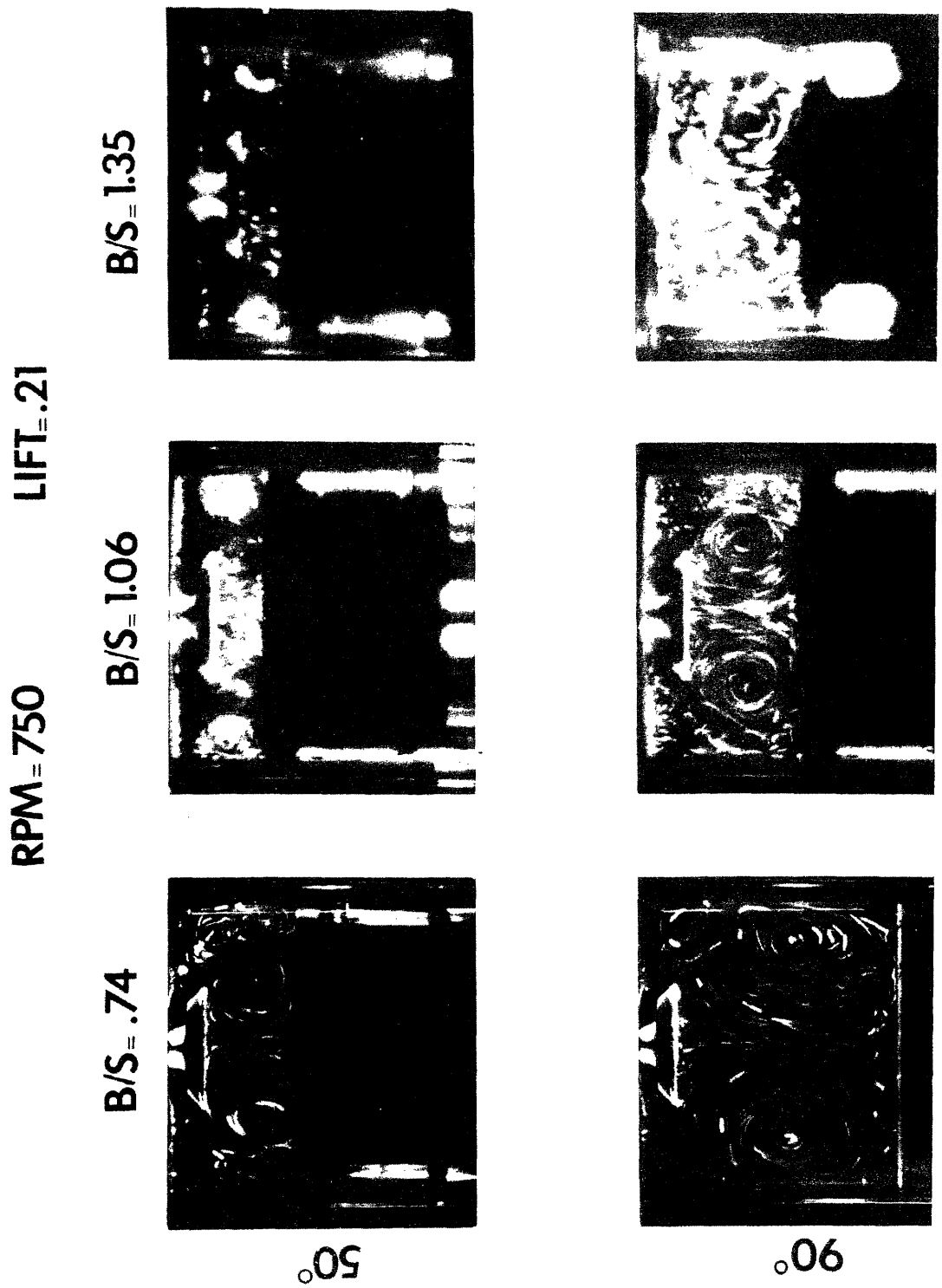

Fig. 15a; Effect of length of stroke on vortex structure; cases 4, 1b and 1a

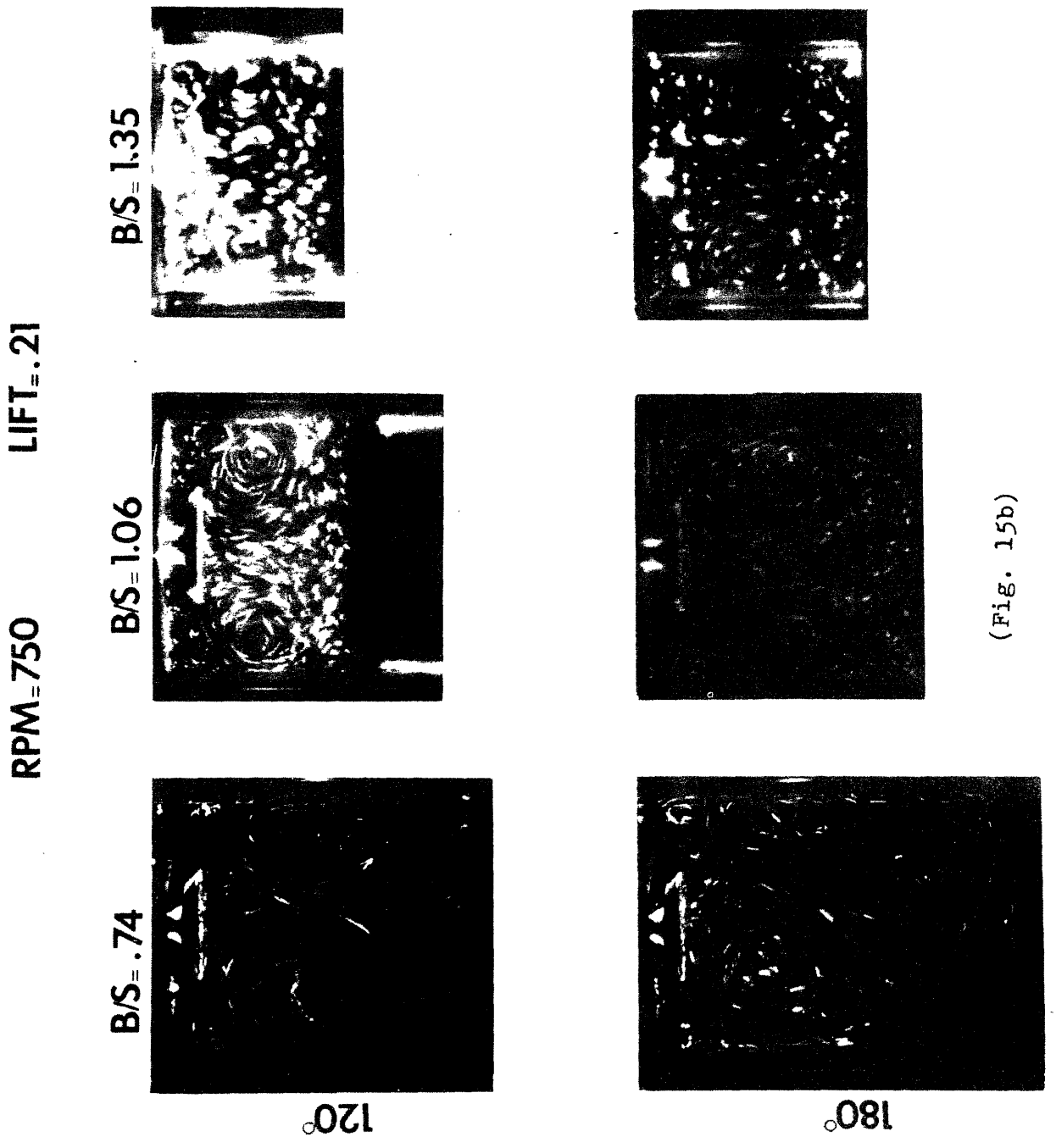

(Fig. 15b)

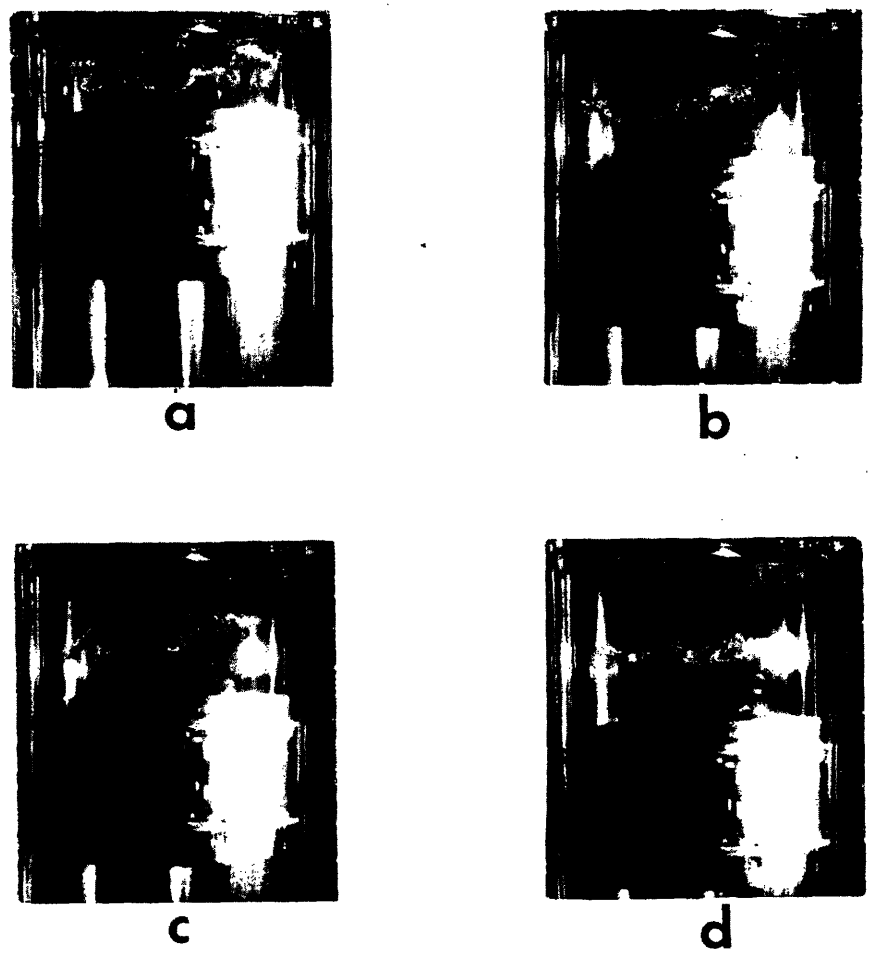

Fig. 16a: Axes of rotation visualized by air bubbles; case 9

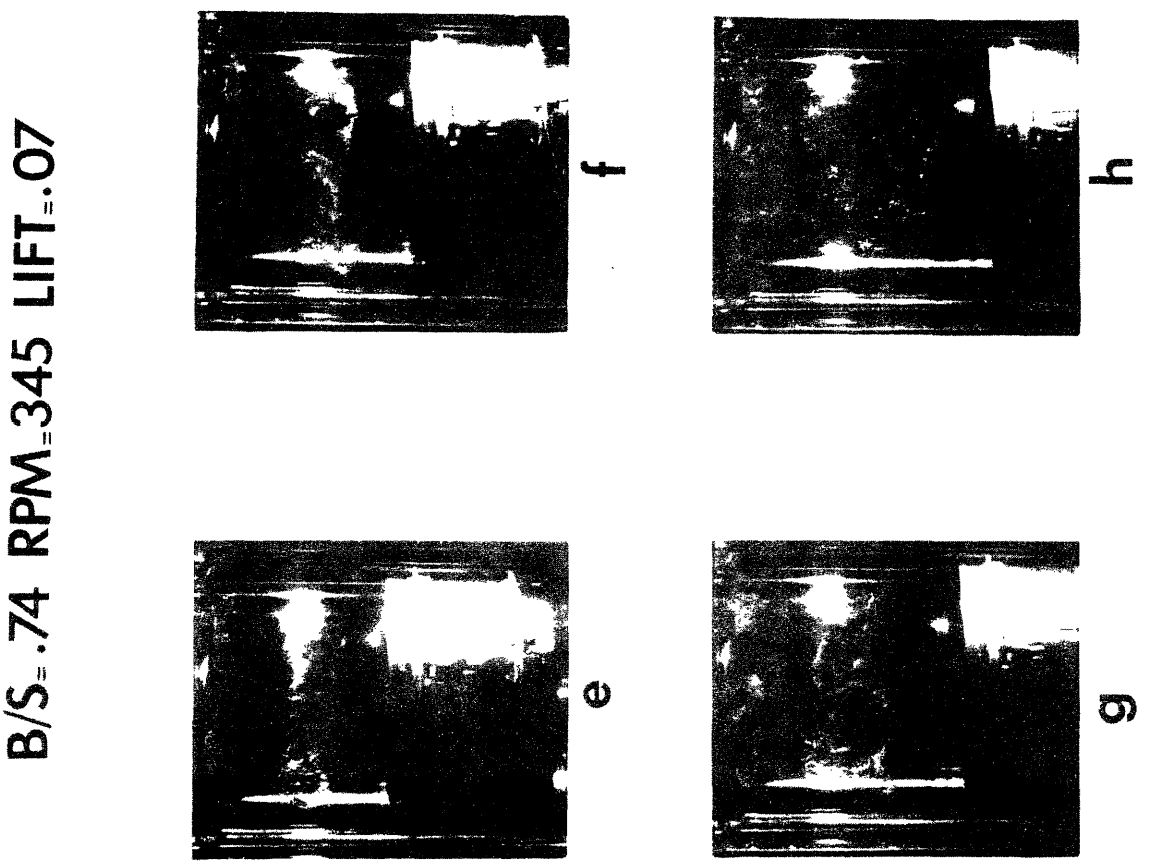

(Fig. 16b)

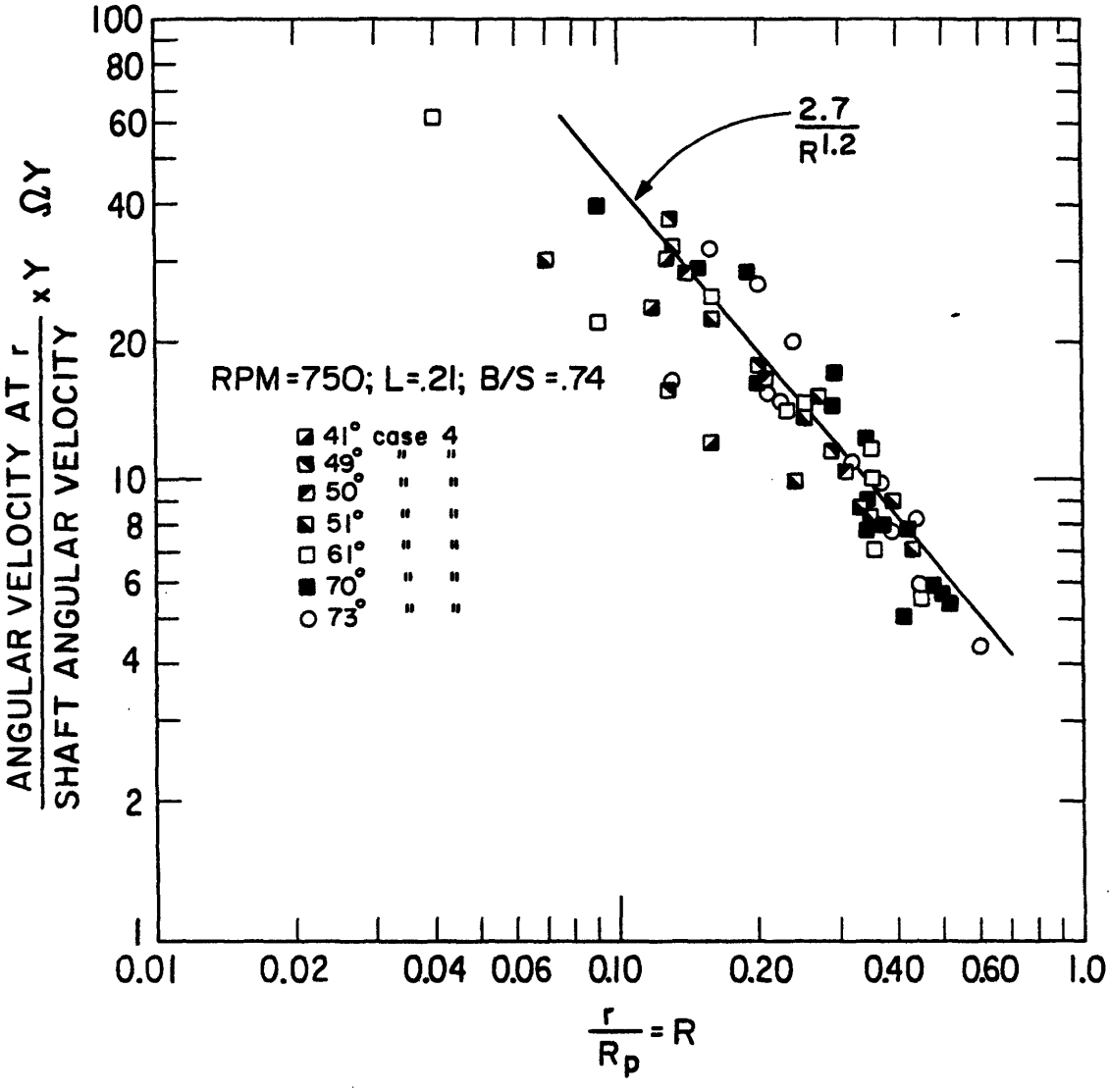

Fig. 17: Variation of nondimensional angular velocity with nondimensional radius, case 4

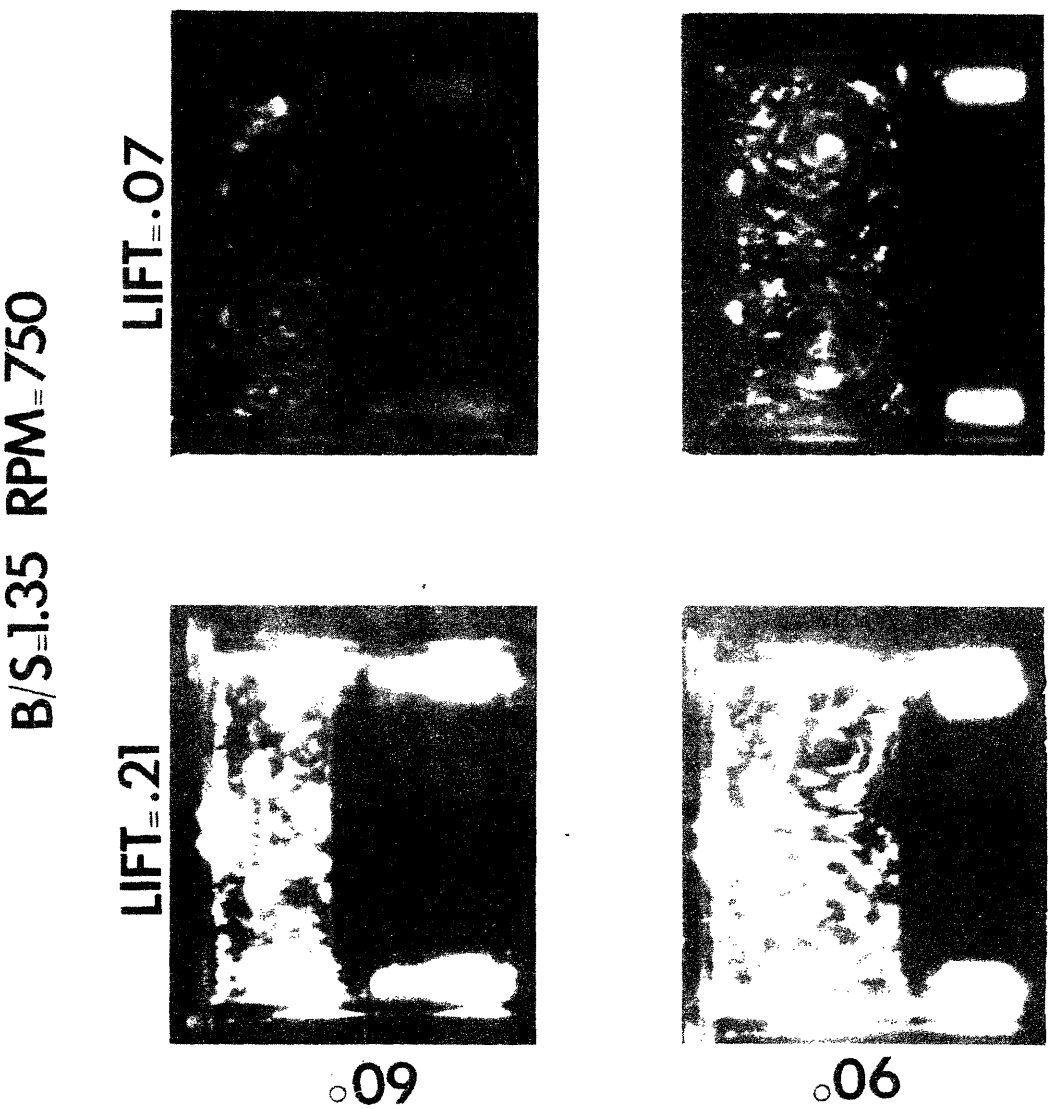

Fig. 18a: Effect of valve lift on vortex structure; cases 1a and 5

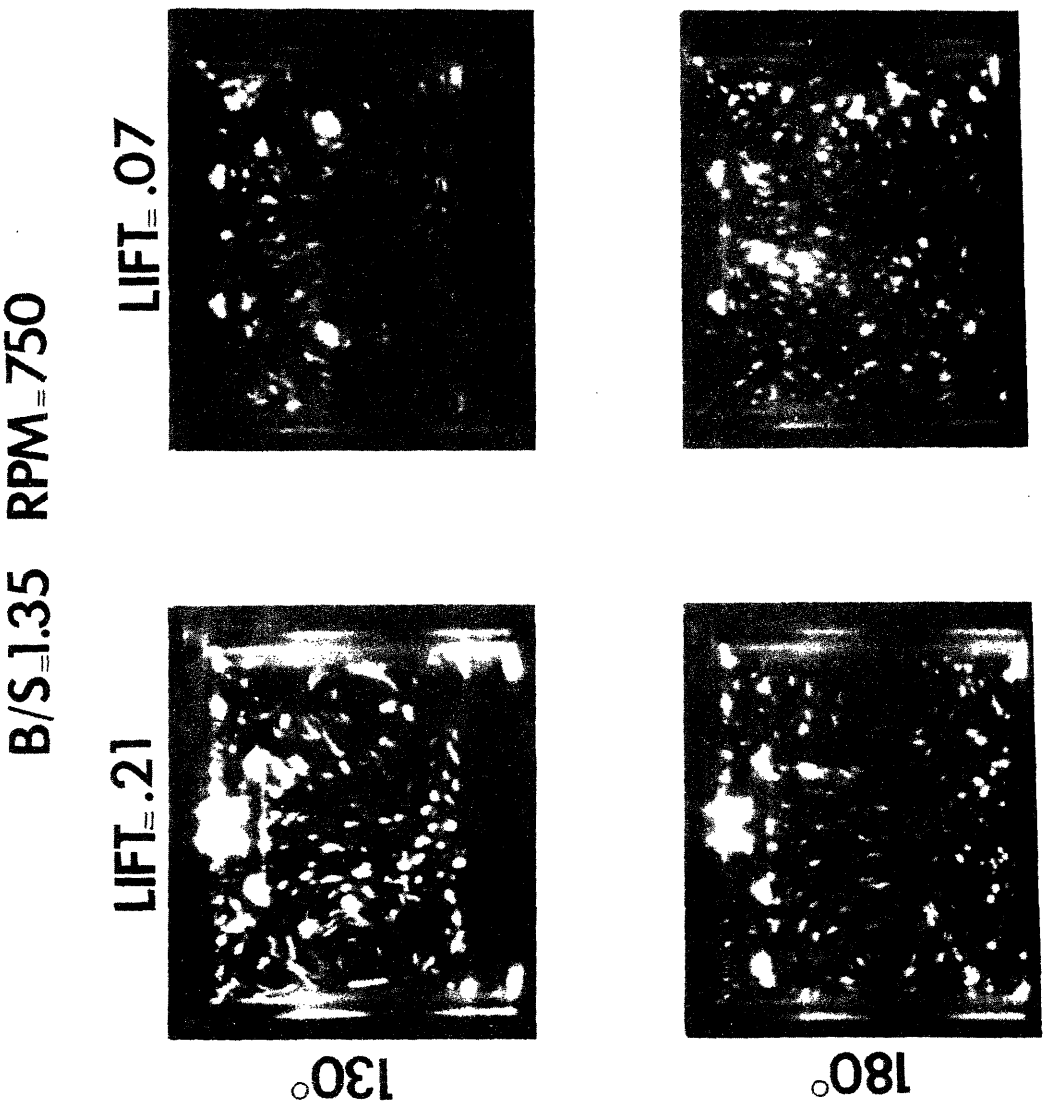

(Fig. 18b)

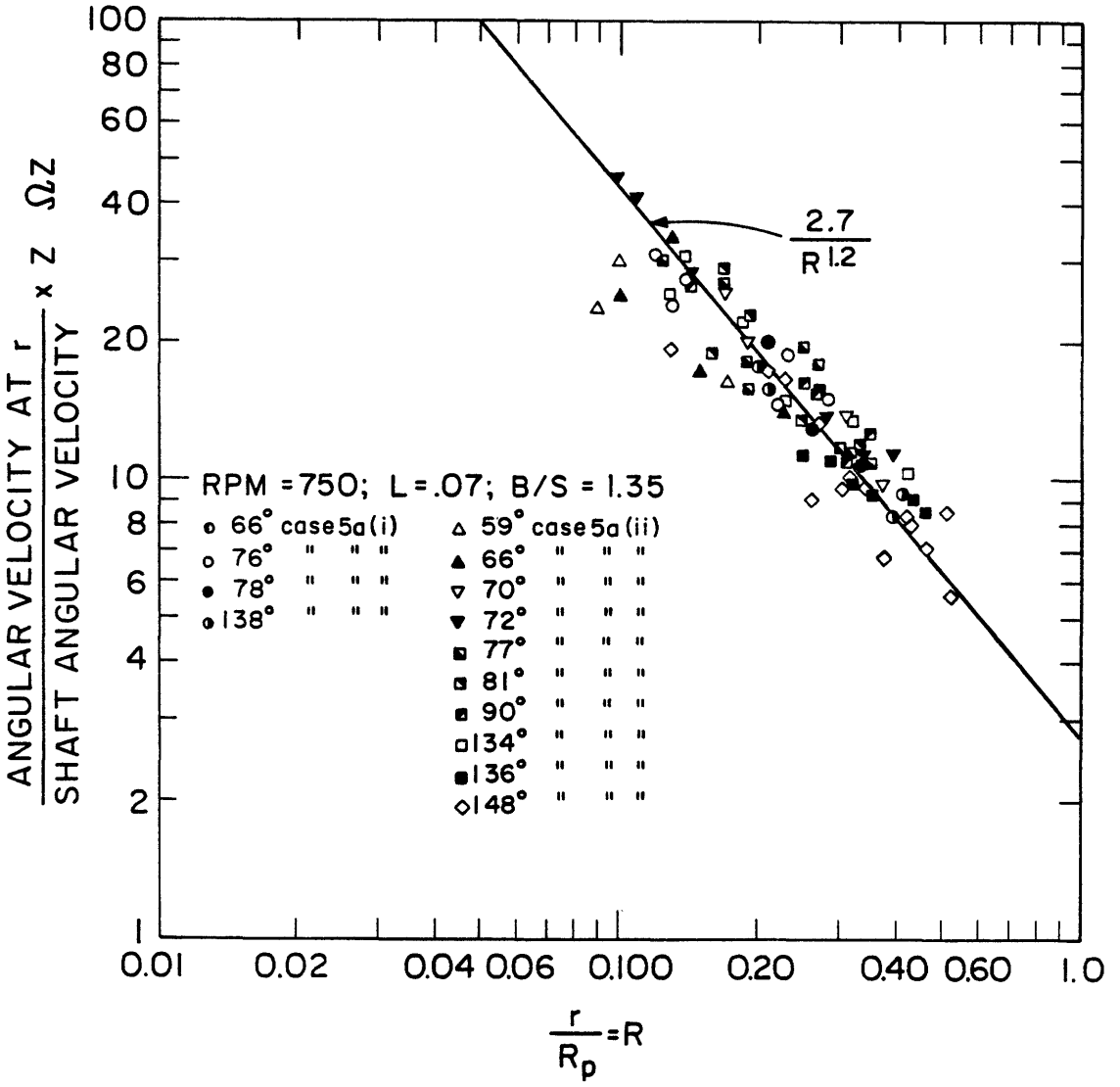

Fig. 19: Variation of nondimensional angular velocity with nondimensional radius; case 5

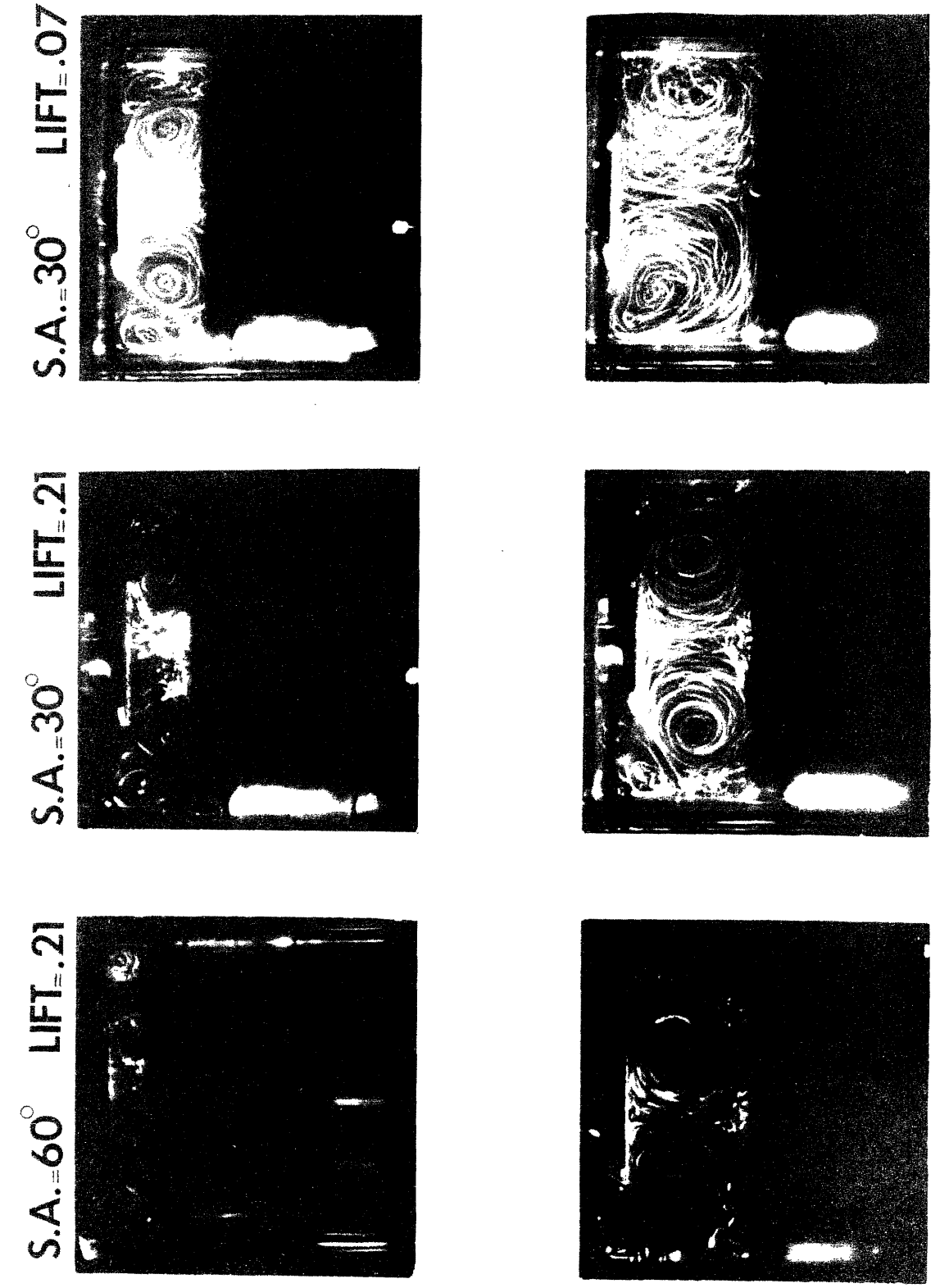

Fig. 20a: Effect of valve seat angle on flow field; cases 6, 7a and 7b

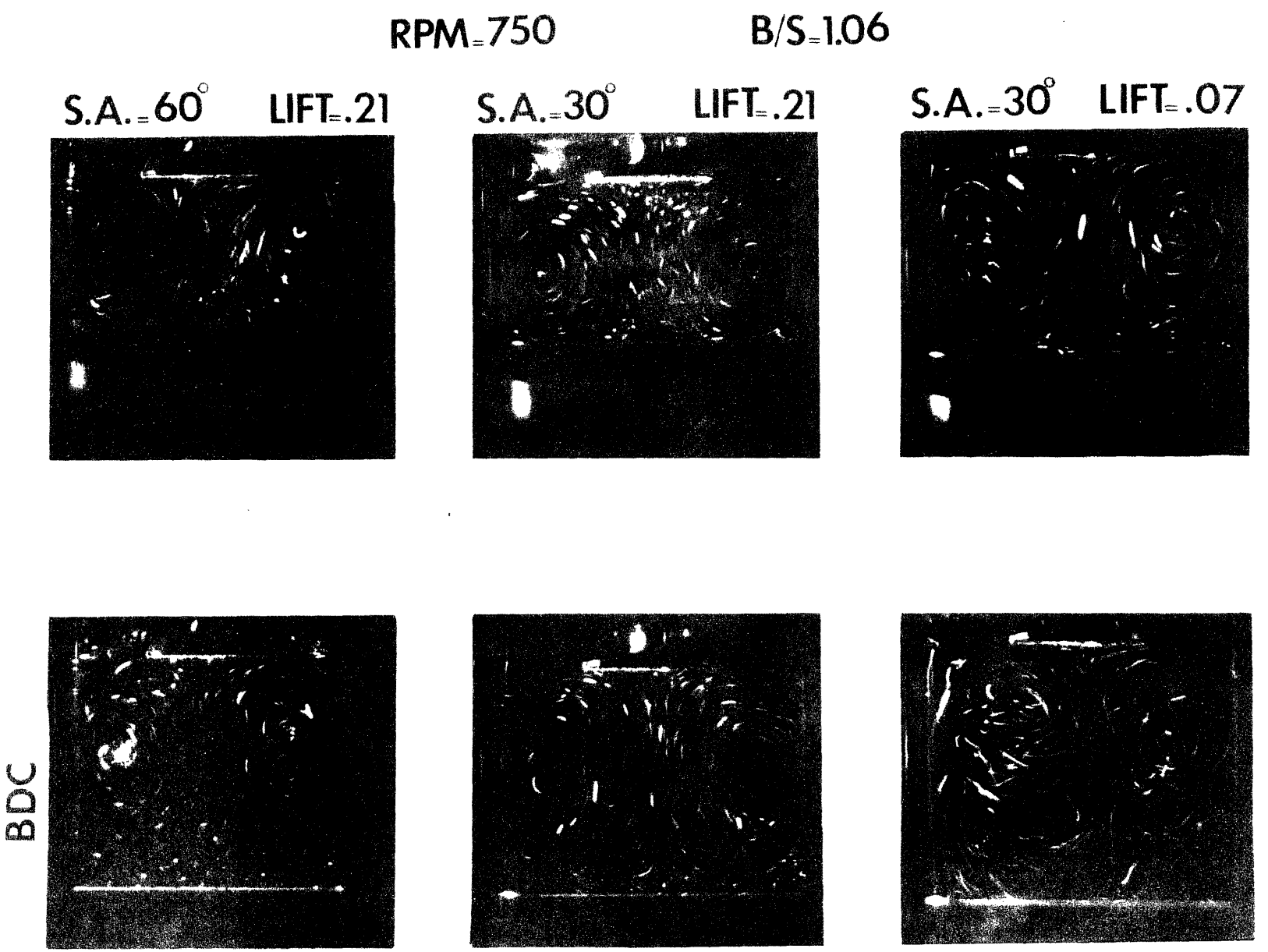

(Fig. 20b)

B/S=1.35 RPM=750 LIFT=.21

(off center valve)

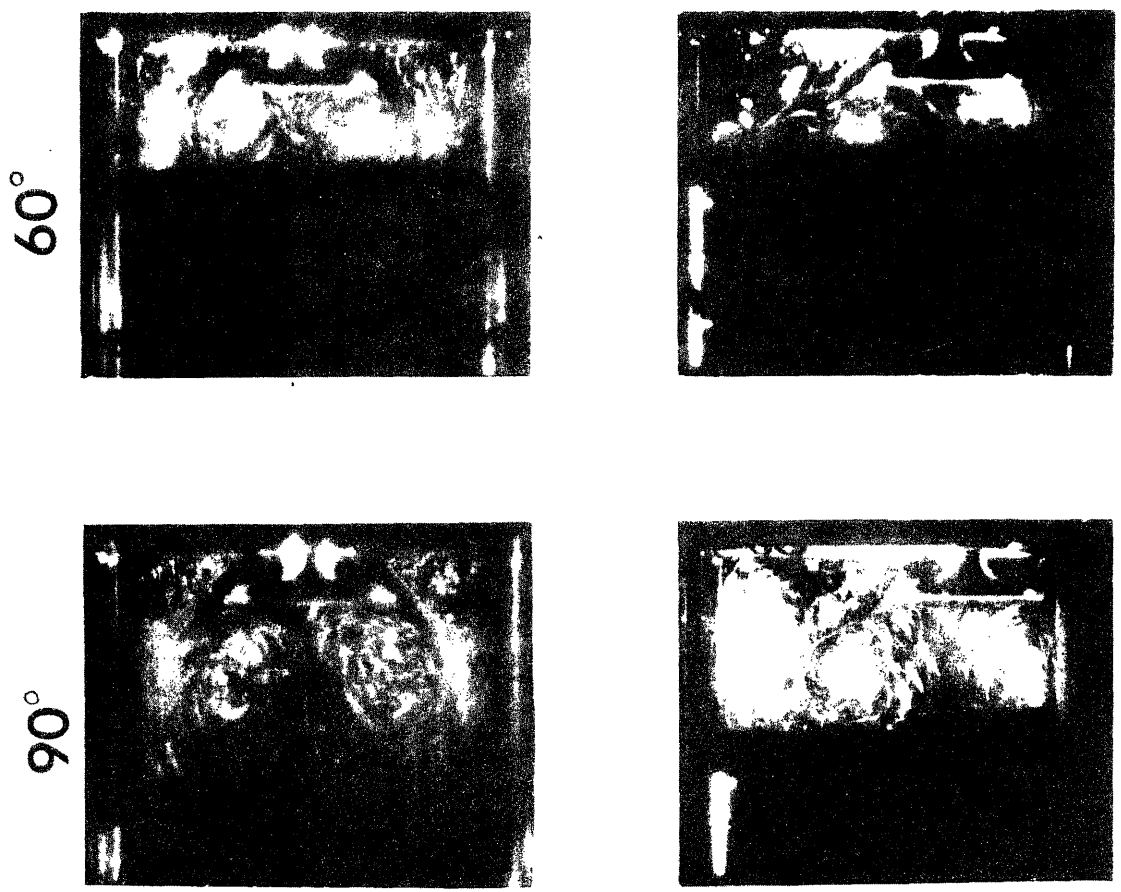

Fig. 21a: Vortex structure in nonaxisymmetric case; plane A left column and plane B right column (see Fig. 6)

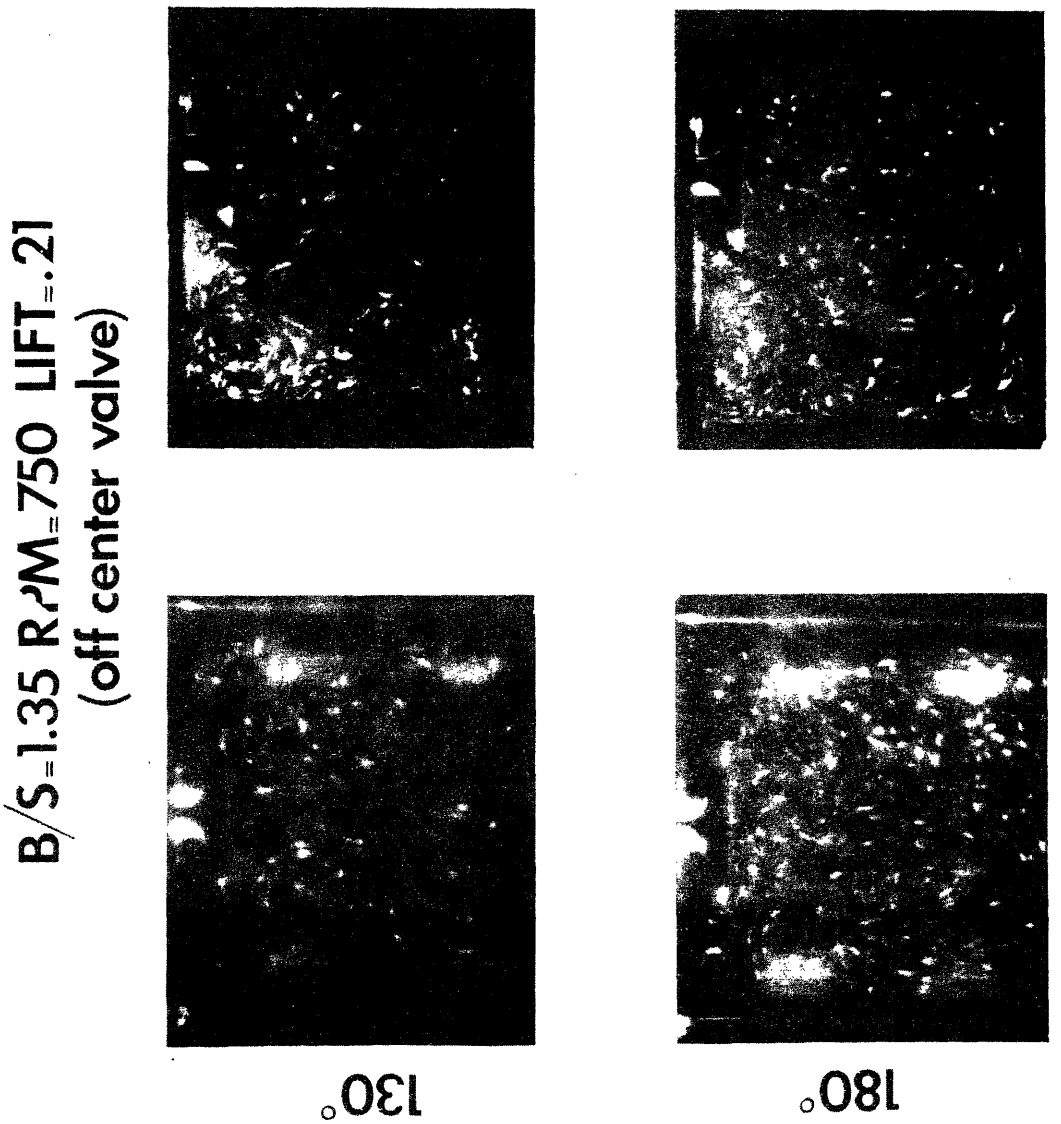

(Fig. 21b)

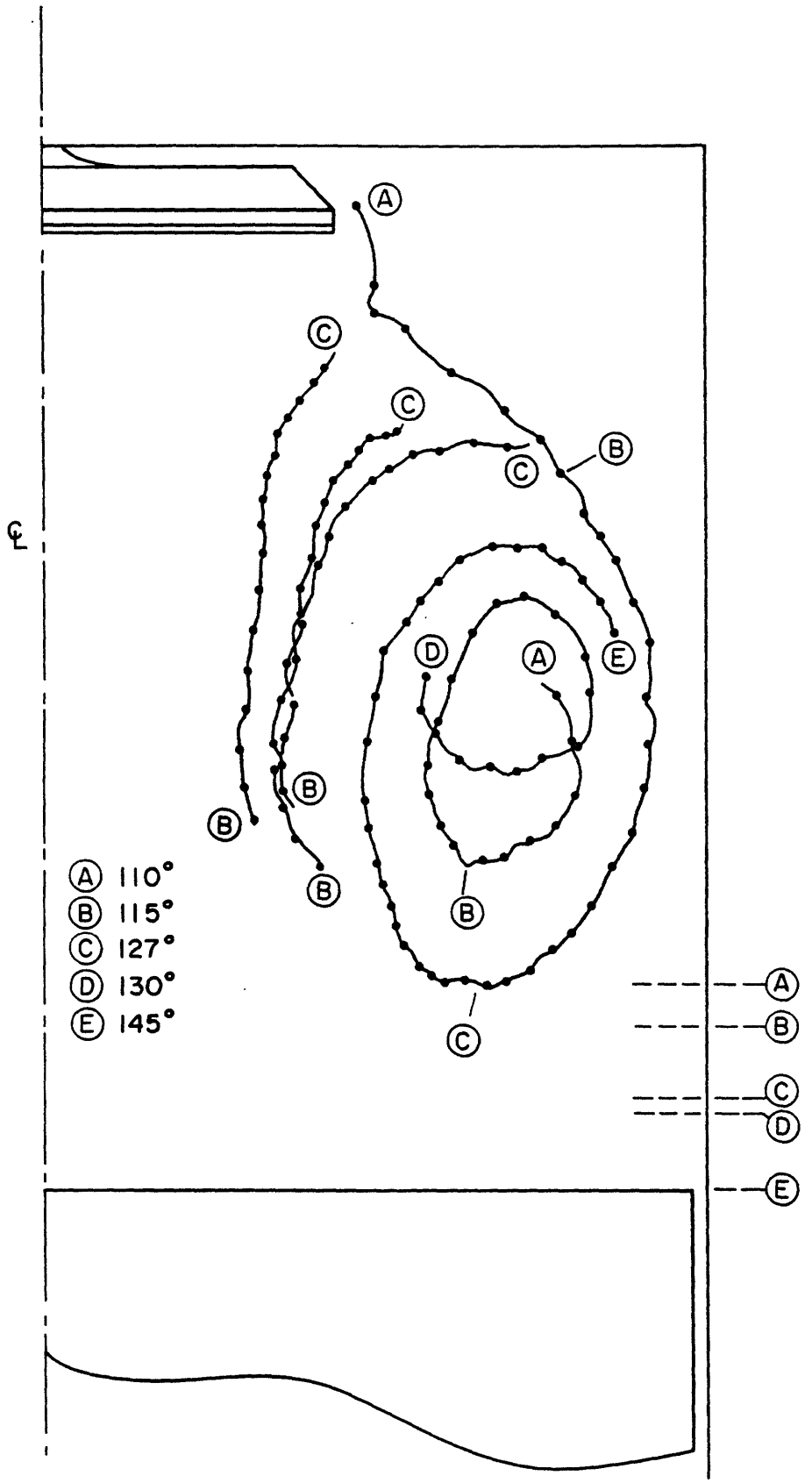

Fig. 22: Particle trajectories